
WAVE SCATTERING AT A RECTANGULAR JUNCTION OF FOUR WAVEGUIDES

Afnan A. Aldosri

School of Information and Physical Sciences
University of Newcastle, Newcastle
afnanabdullahm.aldosri@uon.edu.au

Michael H. Meylan

School of Information and Physical Sciences
University of Newcastle, Newcastle
mike.meylan@newcastle.edu.au

Ben Wilks

School of Information and Physical Sciences
University of Newcastle, Newcastle
ben.wilks@newcastle.edu.au

ABSTRACT

We consider the scattering of linear waves in two dimensions by a rectangular region at the junction of four waveguides. A solution to the frequency domain problem is obtained by exploiting reflective symmetry to reduce the full problem to sub-problems defined on one quadrant of the junction. These sub-problems are solved using the eigenfunction matching method. The solution to the problem on the full region is then recovered from the solutions to the sub-problems, and a scattering matrix for the junction is presented. Finally, the solution in the time domain is constructed as a superposition of the frequency domain solutions and visualised for a range of incident pulses and waveguide geometries.

Keywords Waveguides · Eigenfunction expansion · Wave propagation

1 Introduction

Waveguides have numerous applications across science and technology. They are critical components of electromagnetic and optical systems, acting as communication and sensing technologies [1]. They are also important in other wave-physics scenarios, such as acoustics and water waves [2]. In this latter topic, in which waveguides are more commonly referred to as channels, practical applications include wave flumes and towing tanks used in experimental research. In acoustics, sound propagation through the ducts of air-conditioning systems can also be modelled using waveguides as a framework [3, 4].

The simplest problem to consider is how acoustic, water and electromagnetic waves diffract when encountering parallel half-planes. These investigations have been carried out under various boundary conditions, providing insight into wave behaviour in different contexts, for example, [5, 6, 7, 8], [9, 10, 11] and [12, 13].

Various studies have investigated wave propagation in multi-furcated waveguides under different boundary conditions. For example, bifurcated waveguides have been analyzed for their acoustic wave characteristics in discontinuous structures, considering the effects of soft and hard interfaces [14, 15]. Similarly, research on trifurcated waveguides has explored noise reduction techniques using different porous materials, focusing on their application in silencer modelling [16, 17, 18] and the behaviour of wave scattering in more complex structures, such as pentafurcated ducts, has been studied by [19, 20].

The study of wave scattering has extensively explored scenarios involving one or two step-down or step-up cascading discontinuities, addressing rigid boundary conditions [21, 22, 14, 23, 24, 25], flexible boundary conditions [26, 27], and mixed conditions combining both rigid and flexible [28, 29, 30]. In addition, several studies have focused on fluid-structure interactions at discontinuous interfaces between waveguides, examining how coupled waves scatter under these conditions [26, 31, 32, 33]. In addition, [29] investigated acoustic wave scattering in cavities divided by parallel partitions, while [34] used symmetrical configurations to solve for wave behaviour in a resonator located within a conduit. In contrast, [35, 36] explored asymmetric solutions for wave scattering and validated their findings.

In this paper, we consider the problem of the scattering of waves by a rectangular region at the junction of four waveguides, which has not been considered previously in the literature. The reason for exploring this problem is partly influenced and motivated by quantum graph theory, in which idealised problems of wave scattering on a metric graph can be formulated and intricate scattering networks can be designed, often with nontrivial properties due to local resonance [37, 38]. In this setting, the edges of the graph act as infinitely thin waveguides which support only one mode of propagation. Here, we consider the more general case where the waveguides have a finite thickness and, therefore, support multiple propagating modes. The waveguide junction presented in this paper could be incorporated into a lattice of such junctions, as illustrated in Fig. 1, which could be studied for its locally resonant band structure.

The outline of this paper is as follows: In §2, we formulate the underlying problem, and reduce it to four simpler sub-problems by leveraging the two-fold reflective symmetry of the geometry. In §3, we solve the sub-problems using the eigenfunction matching method (EMM) and present some numerical solutions. In §4, we describe how our solution can be used to obtain the scattering matrix for the junction, which could be used to solve multiple scattering problems. In §5, we describe how to compute the time-domain solution numerically from the frequency-domain solutions. Figures showing the time-domain solution for a range of incident pulses and waveguide geometries are given, with corresponding animations being given in the supplementary material. A brief conclusion is given in §6. For brevity, some peripheral calculations are relegated to the appendices.

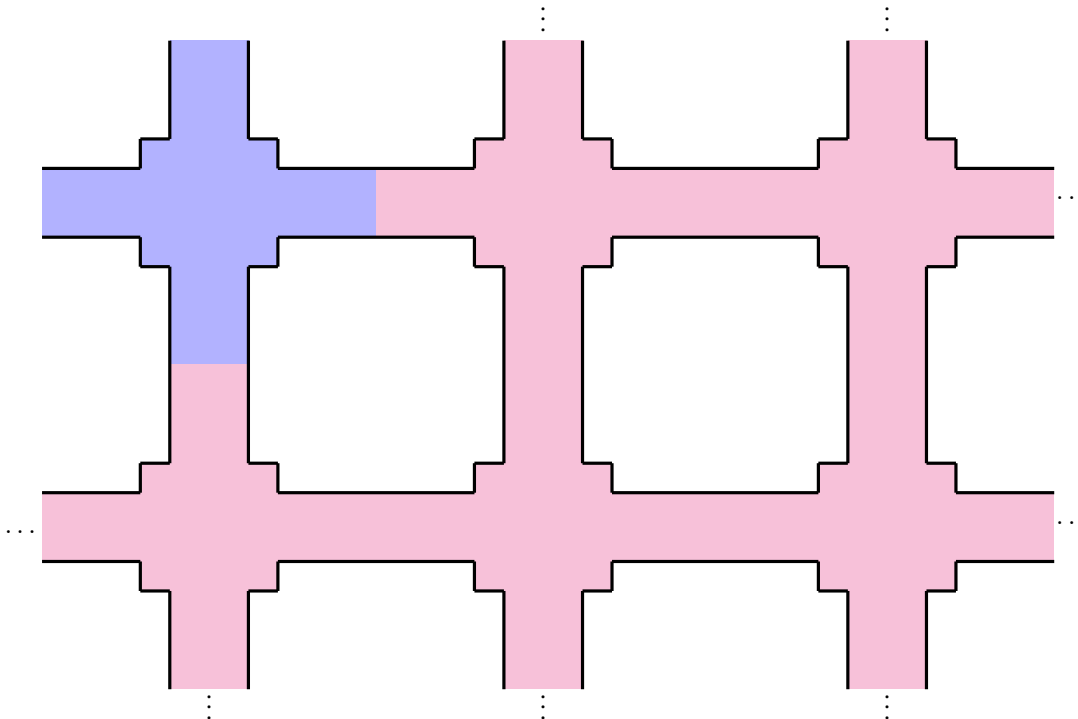


Figure 1: Schematic of a lattice of four-waveguide junctions. This problem, which is a possible extension of our work, is motivated by quantum graph theory, as discussed in the introduction. We will calculate the solution in the region in blue.

2 Mathematical Formulation

We consider the non-dimensionalised two-dimensional wave equation given by

$$\nabla^2 \varphi(x, y, t) - \frac{\partial^2 \varphi(x, y, t)}{\partial t^2} = 0, \quad (1)$$

for $(x, y) \in \Omega$ and $t \in \mathbb{R}$, where ∇^2 denotes the Laplacian and $\Omega \subset \mathbb{R}^2$ is the spatial domain. The problem we consider is a two-dimensional waveguide consisting of four channels connected through a rectangular region, as illustrated in Fig. 2. The horizontal waveguides each have constant width $2a_1$, and the vertical waveguides each have constant width $2a_2$ and are connected by the rectangular region with height and width $2b_1$ and $2b_2$, respectively. The spatial domain is the following union:

$$\begin{aligned} \Omega = & \{(x, y) \mid y \in (-a_1, a_1), x \in (-b_2, -\infty)\} \\ & \cup \{(x, y) \mid y \in (-b_1, -\infty), x \in (-a_2, a_2)\} \\ & \cup \{(x, y) \mid y \in (-a_1, a_1), x \in (b_2, \infty)\} \\ & \cup \{(x, y) \mid y \in (b_1, \infty), x \in (-a_2, a_2)\} \\ & \cup \{(x, y) \mid y \in (-b_1, b_1), x \in (-b_2, b_2)\} \end{aligned} \quad (2)$$

Homogeneous Neumann boundary conditions, which describe no-flow boundaries in the context of water waves or sound hard boundaries in the context of acoustics, are prescribed on the boundaries of the waveguide as follows:

$$\partial_x \varphi = 0, \quad x \in \{-b_2, b_2\}, \quad y \in (-b_1, -a_1) \cup (a_1, b_1), \quad (3a)$$

$$\partial_y \varphi = 0, \quad y \in \{-b_1, b_1\}, \quad x \in (-b_2, -a_2) \cup (a_2, b_2), \quad (3b)$$

$$\partial_y \varphi = 0, \quad y \in \{-a_1, a_1\}, \quad x \in [-b_2, -\infty) \cup [b_2, \infty), \quad (3c)$$

$$\partial_x \varphi = 0, \quad x \in \{-a_2, a_2\}, \quad y \in [-b_1, -\infty) \cup [b_1, \infty). \quad (3d)$$

We express the solution of the wave equation as a continuous superposition of time harmonic functions. The incident wave which is considered here is travelling from left to right

$$\varphi(x, y, t) = \text{Re} \left\{ \int_0^\infty \hat{f}(k) \phi(x, y, k) e^{-ikt} dk \right\}, \quad (4)$$

where $\phi(\cdot, \cdot, k)$ satisfies the Helmholtz equation

$$\nabla^2 \phi(x, y) + k^2 \phi(x, y) = 0, \quad (5)$$

and inherits the boundary conditions (1) satisfied by φ for all $k > 0$. Since wave speed is unity in the non-dimensionalised wave equation, k can be interpreted as both the wavenumber and the angular frequency.

The waveguide has reflective symmetry across the lines $x = 0$ and $y = 0$, which motivates the decomposition of the problem into four different quadrants, as illustrated in Fig. 2. As we will see, the decomposition of the quadrant into rectangular subregions enables a solution to the Helmholtz equation by the method of separation of variables and the eigenfunction matching method.

We now describe how symmetry is used to decompose the full spatial domain into quadrants. If a mode is symmetric about the line $x = 0$, then

$$\phi(x, y) = \phi(-x, y), \quad \forall (x, y) \in \Omega, \quad (6)$$

and its derivative with respect to x must be antisymmetric in x , i.e.

$$\partial_x \phi(x, y) = -\partial_x \phi(-x, y), \quad \forall (x, y) \in \Omega. \quad (7)$$

For $x = 0$, it follows that

$$\partial_x \phi(0, y) = 0, \quad (8)$$

which is a homogeneous Neumann boundary condition. Likewise, if a mode is antisymmetric about the line $x = 0$, then

$$\phi(x, y) = -\phi(-x, y), \quad \forall (x, y) \in \Omega. \quad (9)$$

For $x = 0$, this implies that

$$\phi(0, y) = 0, \quad (10)$$

which is a homogeneous Dirichlet boundary condition. Similar observations are made about modes that are symmetric/antisymmetric about the line $y = 0$. By exploiting symmetry in this way, we will reduce the problem on the full spatial domain to four simpler problems on the principal quadrant $\Omega_P = \{(x, y) \in \Omega \mid x < 0 < y\}$. There are:

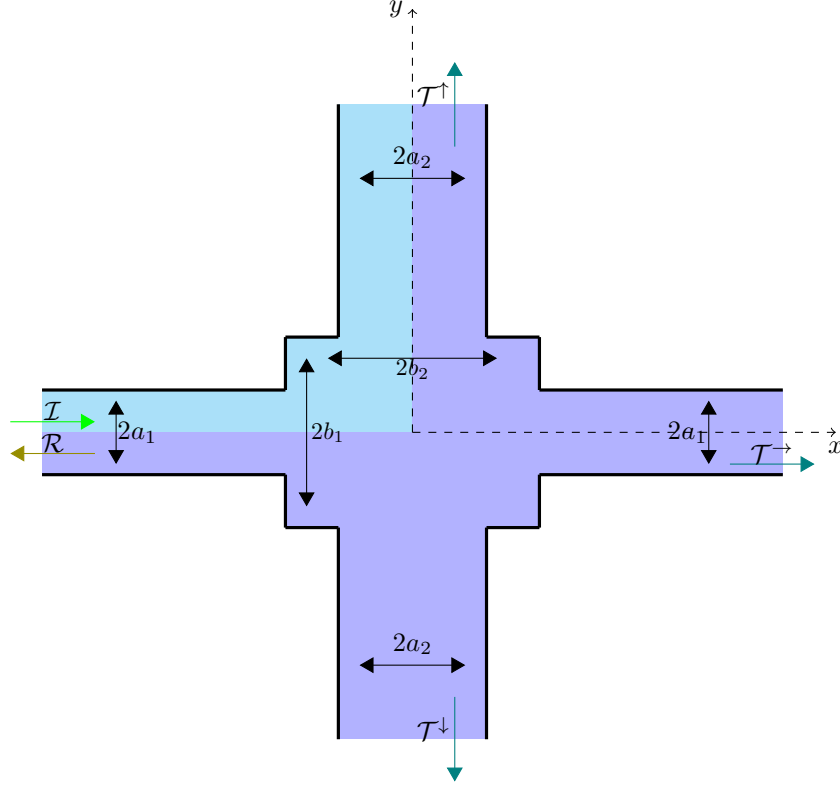


Figure 2: The waveguide geometry illustrates the incident wave, denoted as \mathcal{I} , and the reflected wave, denoted as \mathcal{R} . The transmitted waves are represented as \mathcal{T}^\uparrow , \mathcal{T}^\rightarrow , and \mathcal{T}^\downarrow . We have highlighted the principal quadrant in cyan.

- 1) The Neumann-Neumann problem which satisfies homogeneous Neumann boundary conditions at both $x = 0$ and $y = 0$. We denote the solutions of this problem as $\phi^{\mathcal{N}\mathcal{N}}$. See Fig. 3a.
- 2) The Dirichlet-Dirichlet problem which satisfies homogeneous Dirichlet boundary conditions at $x = 0$ and $y = 0$. We denote the solution of this problem as $\phi^{\mathcal{D}\mathcal{D}}$. See Fig. 3b.
- 3) The Neumann-Dirichlet problem which satisfies a homogeneous Dirichlet boundary condition at $x = 0$ and a homogeneous Neumann boundary condition at $y = 0$. We denote the solution of this problem as $\phi^{\mathcal{N}\mathcal{D}}$. See Fig. 3c.
- 4) The Dirichlet-Neumann problem which satisfies a homogeneous Dirichlet boundary condition at $y = 0$ and a homogeneous Neumann boundary condition at $x = 0$. We denote the solution of this problem as $\phi^{\mathcal{D}\mathcal{N}}$. See Fig. 3d.

All four problems also satisfy homogeneous Neumann boundary conditions on the physical boundary inherited from (3).

We will solve each of the four problems above, assuming a unit-amplitude plane wave incident from $x = -\infty$. The solution for a unit-amplitude plane wave incident from $x = -\infty$ in the full domain can be reconstructed from these solutions in the principal quadrant. If the incident wave is symmetric about the line $y = 0$, then the reconstructed solution is

$$\phi(x, y) = \begin{cases} \frac{1}{2}(\phi^{\mathcal{N}\mathcal{N}}(x, y) + \phi^{\mathcal{D}\mathcal{N}}(x, y)), & \text{if } x < 0, \quad y > 0, \\ \frac{1}{2}(\phi^{\mathcal{N}\mathcal{N}}(-x, y) - \phi^{\mathcal{D}\mathcal{N}}(-x, y)), & \text{if } x > 0, \quad y > 0, \\ \frac{1}{2}(\phi^{\mathcal{N}\mathcal{N}}(x, -y) + \phi^{\mathcal{D}\mathcal{N}}(x, -y)), & \text{if } x < 0, \quad y < 0, \\ \frac{1}{2}(\phi^{\mathcal{N}\mathcal{N}}(-x, -y) - \phi^{\mathcal{D}\mathcal{N}}(-x, -y)), & \text{if } x > 0, \quad y < 0. \end{cases} \quad (11)$$

Otherwise, if the incident wave is antisymmetric about the line $x = 0$, then the reconstructed solution is

$$\phi(x, y) = \begin{cases} \frac{1}{2}(\phi^{\mathcal{DD}}(x, y) + \phi^{\mathcal{ND}}(x, y)), & \text{if } x < 0, \quad y > 0, \\ \frac{1}{2}(\phi^{\mathcal{DD}}(-x, y) - \phi^{\mathcal{ND}}(-x, y)), & \text{if } x > 0, \quad y > 0, \\ \frac{1}{2}(\phi^{\mathcal{DD}}(x, -y) + \phi^{\mathcal{ND}}(x, -y)), & \text{if } x < 0, \quad y < 0, \\ \frac{1}{2}(\phi^{\mathcal{DD}}(-x, -y) - \phi^{\mathcal{ND}}(-x, -y)), & \text{if } x > 0, \quad y < 0. \end{cases} \quad (12)$$

2.1 Separation of variables

In order to apply the method of separation of variables, the principal quadrant Ω_P is further decomposed into $\Omega_1 := \{-\infty < x \leq -b_2, \quad 0 < y \leq -a_1\}$, $\Omega_2 := \{0 < x \geq -b_2, \quad 0 < y \leq b_1\}$, and $\Omega_3 := \{0 > x \geq -a_2, \quad b_1 \leq y < \infty\}$, as illustrated in Fig. 3a. A scattering problem in the quadrant is posed by considering an incident wave propagating along Ω_1 from $x = -\infty$ as shown in Fig. 3a. The next step is to define the expansions of the eigenfunction in each mode and the orthogonality relation in each region of the channel based on the boundary conditions. Subsequently, these expansions are matched using the following continuity of the pressure and normal velocity conditions:

$$\lim_{x \rightarrow -b_2^+} \phi^{\mathcal{NN}}(x, y) = \lim_{x \rightarrow -b_2^-} \phi^{\mathcal{NN}}(x, y), \quad x = -b_2, \quad y \in (0, a_1), \quad (13a)$$

$$\lim_{y \rightarrow b_1^+} \phi^{\mathcal{NN}}(x, y) = \lim_{y \rightarrow b_1^-} \phi^{\mathcal{NN}}(x, y), \quad y = b_1, \quad x \in (-a_2, 0). \quad (13b)$$

and

$$\lim_{x \rightarrow -b_2^+} \frac{\partial \phi^{\mathcal{NN}}(x, y)}{\partial x} = \begin{cases} 0, & \text{if } y \in (a_1, b_1), \\ \lim_{x \rightarrow -b_2^-} \frac{\partial \phi^{\mathcal{NN}}(x, y)}{\partial x}, & \text{if } y \in (0, a_1). \end{cases} \quad (14a)$$

$$\lim_{y \rightarrow b_1^+} \frac{\partial \phi^{\mathcal{NN}}(x, y)}{\partial y} = \begin{cases} 0, & \text{if } x \in (-b_2, -a_2), \\ \lim_{y \rightarrow b_1^-} \frac{\partial \phi^{\mathcal{NN}}(x, y)}{\partial y}, & \text{if } x \in (-a_2, 0). \end{cases} \quad (14b)$$

Identical matching condition hold for $\phi^{\mathcal{DD}}$, $\phi^{\mathcal{ND}}$ and $\phi^{\mathcal{DN}}$.

Next, the details of the Neumann-Neumann problem will be given in full, with details of the remaining three sub-problems being relegated to A.

2.2 Neumann-Neumann solutions

The Helmholtz equation (5) is solved subject to both physical boundary conditions

$$\phi_y^{\mathcal{NN}}(x, y) = 0, \quad y = a_1, b_1, \quad x \in (-a_2, -\infty), \quad (15a)$$

$$\phi_x^{\mathcal{NN}}(x, y) = 0, \quad x = -a_2, -b_2, \quad y \in (a_1, \infty), \quad (15b)$$

and artificial boundary conditions

$$\phi_y^{\mathcal{NN}}(x, y) = 0, \quad y = 0, \quad x \in (0, -\infty), \quad (16a)$$

$$\phi_x^{\mathcal{NN}}(x, y) = 0, \quad x = 0, \quad y \in (0, \infty), \quad (16b)$$

as shown in Fig. 3a. The solution is obtained in piecewise form as

$$\phi^{\mathcal{NN}}(x, y) = \begin{cases} \phi_1^{\mathcal{NN}}(x, y), & (x, y) \in \Omega_1, \\ \phi_2^{\mathcal{NN}}(x, y) + \phi_2^{\mathcal{NN}}(x, y), & (x, y) \in \Omega_2, \\ \phi_3^{\mathcal{NN}}, & (x, y) \in \Omega_3. \end{cases} \quad (17)$$

The solution in region Ω_1 that satisfies (5), (15a) and (15b) is written as

$$\phi_1^{\mathcal{NN}}(x, y) = e^{i\bar{\beta}_p(x+b_2)} \Phi_p(y) + \sum_{n=0}^{\infty} A_n^{\mathcal{NN}} e^{-i\bar{\beta}_n(x+b_2)} \Phi_n(y). \quad (18)$$

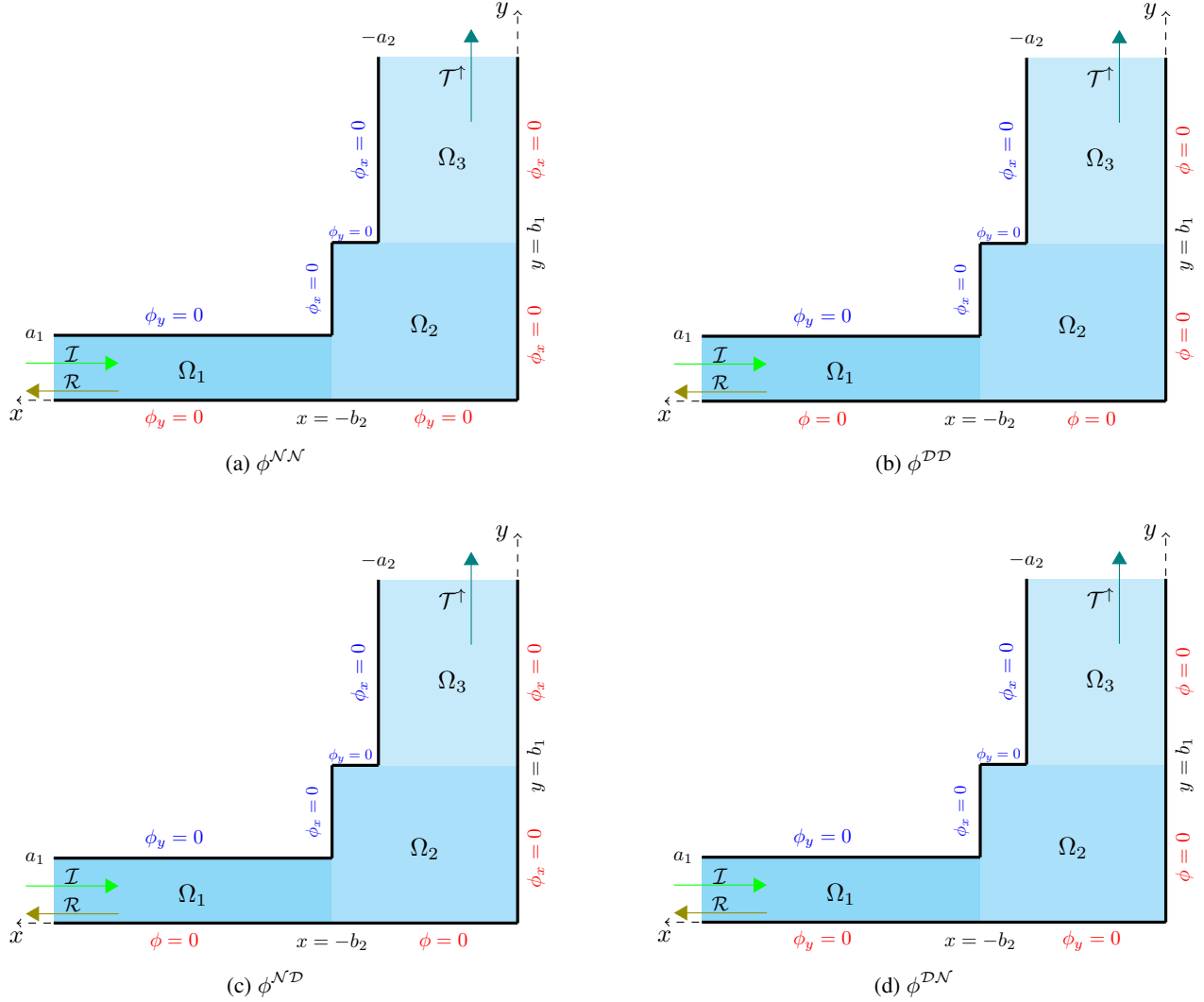


Figure 3: Waveguide geometries showing the boundary conditions satisfied by (a) $\phi^{\mathcal{N}\mathcal{N}}$, (b) $\phi^{\mathcal{D}\mathcal{D}}$, (c) $\phi^{\mathcal{N}\mathcal{D}}$, and (d) $\phi^{\mathcal{D}\mathcal{N}}$. Physical boundary conditions are denoted in blue, whereas artificial boundary conditions are denoted in red.

Here, $\bar{\beta}_n = \sqrt{k^2 - \beta_n^2}$ is the wavenumber of the n th reflected mode in which $\beta_n = n\pi/a_1$ is the eigenvalue for all $n \in \mathbb{N}_0$. The corresponding eigenfunctions $\Phi_n(y) = \cos(\beta_n y)$ satisfies the orthogonality relation

$$I_{mn}(a_1) = \int_0^{a_1} \Phi_n(y)\Phi_m(y)dy = \kappa_m a_1 \delta_{mn}, \quad (19)$$

where δ_{mn} is Kronecker delta and κ_m is defined as

$$\kappa_m = \begin{cases} 1, & \text{if } m = n = 0, \\ \frac{1}{2}, & \text{if } m = n \neq 0, \\ 0, & \text{otherwise.} \end{cases}$$

Note that the first term in (18) describes the incident wave, while the second term describes the reflected wave in which $A_n^{\mathcal{N}\mathcal{N}}$ is the amplitude of the n th reflected mode.

In region Ω_2 , a superposition of two series is required to satisfy the boundary and matching conditions. Thus, the solutions in region Ω_2 which satisfies (5), (15a), (15b) and (16b) and then (5), (15a), (15b) and (16a) respectively are

$$\phi_2^{\mathcal{N}\mathcal{N}}(x, y) = \sum_{n=0}^{\infty} B_n^{\mathcal{N}\mathcal{N}} \left(\frac{\cosh(i\bar{\alpha}_n x)}{\cosh(-i\bar{\alpha}_n b_2)} \right) \Gamma_n(y), \quad (20)$$

$$\phi_2^{\mathcal{NN}}(x, y) = \sum_{n=0}^{\infty} C_n^{\mathcal{NN}} \left(\frac{\cosh(i\bar{\eta}'_n y)}{\cosh(i\bar{\eta}'_n b_1)} \right) \Upsilon_n(x). \quad (21)$$

Here, $\bar{\alpha}_n = \sqrt{k^2 - \alpha_n^2}$ and $\bar{\eta}'_n = \sqrt{k^2 - \eta_n'^2}$ are the wavenumbers of the n th transmitted mode, in which $\alpha_n = n\pi/b_1$ and $\eta_n' = n\pi/b_2$ are the eigenvalues for $n = 0, 1, 2, \dots$. The corresponding eigenfunctions $\Gamma_n(y) = \cos(\alpha_n y)$ and $\Upsilon_n(x) = \cos(\eta_n' x)$ satisfy the orthogonality relation on their respective domains of definition. The solution in region Ω_3 that satisfies (5), (16a), and (16b) is

$$\phi_3^{\mathcal{NN}}(x, y) = \sum_{n=0}^{\infty} D_n^{\mathcal{NN}} e^{i\bar{\eta}_n(y-b_1)} \aleph_n(x). \quad (22)$$

Here $\bar{\eta}_n = \sqrt{k^2 - \eta_n^2}$ is the wavenumber of the n th transmitted mode in which $\eta_n = n\pi/a_2$ is the eigenvalue for $n \in \mathbb{N}_0$. The corresponding eigenfunction $\aleph_n(x) = \cos(\eta_n x)$ satisfies the orthogonality on their respective domains of definition. Note that $D_n^{\mathcal{NN}}$ in (22) is the amplitude of the transmitted mode coefficient.

2.3 Dirichlet-Dirichlet solutions

The Helmholtz equation (5) is solved subject to physical boundary conditions

$$\phi_y^{\mathcal{DD}}(x, y) = 0, \quad y = a_1, b_1, \quad x \in (-a_2, -\infty), \quad (23a)$$

$$\phi^{\mathcal{DD}}(x, y) = 0, \quad y = 0, \quad x \in (0, -\infty), \quad (23b)$$

and artificial boundary conditions

$$\phi_x^{\mathcal{DD}}(x, y) = 0, \quad x = -b_2, -a_2, \quad y \in (a_1, \infty) \quad (24a)$$

$$\phi^{\mathcal{DD}}(x, y) = 0, \quad x = 0, \quad y \in (0, \infty), \quad (24b)$$

as shown in Fig. 3b. The solution, in this case, is obtained in piecewise form as

$$\phi^{\mathcal{DD}}(x, y) = \begin{cases} \phi_1^{\mathcal{DD}}(x, y), & (x, y) \in \Omega_1, \\ \phi_2^{\mathcal{DD}}(x, y) + \phi_2'^{\mathcal{DD}}(x, y), & (x, y) \in \Omega_2, \\ \phi_3^{\mathcal{DD}}, & (x, y) \in \Omega_3. \end{cases} \quad (25)$$

The solution in region Ω_1 which satisfies (5), (23a), and (23b) is

$$\phi_1^{\mathcal{DD}}(x, y) = e^{i\bar{\gamma}_p(x+b_2)} \tilde{\Phi}_p(y) + \sum_{n=1}^{\infty} A_n^{\mathcal{DD}} e^{-i\bar{\gamma}_n(x+b_2)} \tilde{\Phi}_n(y). \quad (26)$$

Here, $\bar{\gamma}_n = \sqrt{k^2 - \gamma_n^2}$, $\gamma_n = (2n+1)\pi/2a_1$ for $n = 0, 1, 2, \dots$ and $\tilde{\Phi}_n(y) = \sin(\gamma_n y)$ satisfy the orthogonality

$$\hat{I}_{mn}(a_1) = \int_0^{a_1} \tilde{\Phi}_n(y) \tilde{\Phi}_m(y) dy = \frac{1}{2} a_1 \delta_{mn}, \quad (27)$$

The first term in (26) is the incident wave, and the second term is the reflected field in which $A_n^{\mathcal{DD}}$ is the amplitude of the n th reflected mode. The solutions in region Ω_2 that satisfy (5), (23a), (23b), and (24b) and then (5), (23b), (24a) and (24b) respectively are

$$\phi_2^{\mathcal{DD}}(x, y) = \sum_{n=1}^{\infty} B_n^{\mathcal{DD}} \left(\frac{\sinh(i\bar{\lambda}_n x)}{\sinh(-i\bar{\lambda}_n b_2)} \right) \tilde{\Gamma}_n(y), \quad (28)$$

$$\phi_2'^{\mathcal{DD}}(x, y) = \sum_{n=1}^{\infty} C_n^{\mathcal{DD}} \left(\frac{\sinh(i\bar{\zeta}_n y)}{\sinh(i\bar{\zeta}_n b_1)} \right) \tilde{\Upsilon}_n(x), \quad (29)$$

where $\bar{\lambda}_n = \sqrt{k^2 - \lambda_n^2}$, $\bar{\zeta}_n = \sqrt{k^2 - \zeta_n^2}$, $\lambda_n = (2n+1)\pi/2b_2$, $\zeta_n = (2n+1)\pi/2b_2$ and $\tilde{\Gamma}_n(y) = \sin(\lambda_n y)$ and $\tilde{\Upsilon}_n(x) = \sin(\zeta_n x)$ satisfy the orthogonality. The solution in region Ω_3 that satisfy (5), (24a), and (24b) is

$$\phi_3^{\mathcal{DD}}(x, y) = \sum_{n=1}^{\infty} D_n^{\mathcal{DD}} e^{i\bar{\zeta}'_n(y-b_1)} \tilde{\aleph}_n(x), \quad (30)$$

where $\bar{\zeta}'_n = \sqrt{k^2 - \zeta_n'^2}$, $\zeta_n' = (2n+1)\pi/2a_2$, for $n = 0, 1, 2, \dots$ and $\tilde{\aleph}_n(x) = \sin(\zeta_n' x)$ satisfy the orthogonality.

Note that $D_n^{\mathcal{DD}}$ in (30) is the amplitude of the transmitted mode coefficient.

2.4 Neumann-Dirichlet solutions

The Helmholtz equation (5) is solved subject to physical boundary conditions

$$\phi_y(x, y) = 0, \quad y = b_1, \quad x \in (-b_2, -a_2), \quad (31a)$$

$$\phi_x(x, y) = 0, \quad x = -b_2, \quad y \in (a_1, b_1), \quad (31b)$$

and artificial boundary conditions

$$\phi_x(x, y) = 0, \quad x = 0, \quad y \in (0, b_1), \quad (32a)$$

$$\phi(x, y) = 0, \quad y = 0, \quad x \in (0, -b_2). \quad (32b)$$

as shown in Fig. 3c. The solution in Ω_1 is of the form given in (26). The solutions in region Ω_2 that satisfy (5), (31a), (31b), and (32b) and then satisfy (5), (31a), (31b), and (32a) are

$$\phi_2^{\mathcal{ND}}(x, y) = \sum_{n=0}^{\infty} B_n^{\mathcal{ND}} \left(\frac{\cosh(i\bar{\lambda}_n x)}{\cosh(-i\bar{\lambda}_n b_2)} \right) \tilde{\Gamma}_n(y), \quad (33)$$

$$\phi_2^{\mathcal{ND}}(x, y) = \sum_{n=1}^{\infty} C_n^{\mathcal{ND}} \left(\frac{\sinh(i\bar{\eta}'_n y)}{\sinh(i\bar{\eta}'_n b_1)} \right) \Upsilon_n(x), \quad (34)$$

Additionally, the solution in Ω_3 is of the form given in (22), where the definitions of the eigenvalues and the eigenfunctions remain unchanged.

2.5 Dirichlet-Neumann solutions

The Helmholtz equation (5) is solved subject to physical boundary conditions

$$\phi_y(x, y) = 0, \quad y = b_1, \quad x \in (-b_2, -a_2), \quad (35a)$$

$$\phi_x(x, y) = 0, \quad x = -b_2, \quad y \in (a_1, b_1), \quad (35b)$$

and artificial boundary conditions

$$\phi_y(x, y) = 0, \quad y = 0, \quad x \in (-b_2, 0), \quad (36a)$$

$$\phi(x, y) = 0, \quad x = 0, \quad y \in (b_1, 0). \quad (36b)$$

as shown in Fig. 3d. The solution in Ω_1 is of the form given in (18). The solutions in region Ω_2 that satisfy (5), (35a), (36a), and (36b) and then satisfy (5), (35a), (35b), and (36b) are

$$\phi_2^{\mathcal{DN}}(x, y) = \sum_{n=0}^{\infty} B_n^{\mathcal{DN}} \left(\frac{\sinh(i\bar{\alpha}_n x)}{\sinh(-i\bar{\alpha}_n b_2)} \right) \Gamma_n(y), \quad (37)$$

$$\phi_2^{\mathcal{DN}}(x, y) = \sum_{n=0}^{\infty} C_n^{\mathcal{DN}} \left(\frac{\cosh(i\bar{\zeta}_n y)}{\cosh(i\bar{\zeta}_n b_1)} \right) \tilde{\Upsilon}_n(x). \quad (38)$$

The solution in Ω_3 is of the form given in (30). Where there is no change in the eigenvalues and the eigenfunctions.

Next, we will describe how the unknown coefficients are determined numerically using the eigenfunction matching method.

3 Numerical solution using eigenfunction matching

Details of the eigenfunction matching method are given in full for the Neumann-Neumann problem, with those of the remaining three subproblems being relegated to the appendix. After substituting the general solutions (18), (20) and (21), the matching conditions at the interface $x = -b_2$, (13a) becomes

$$\Phi_p(y) + \sum_{n=0}^{\infty} A_n^{\mathcal{NN}} \Phi_n(y) = \sum_{n=0}^{\infty} B_n^{\mathcal{NN}} \Gamma_n(y) + \sum_{n=0}^{\infty} C_n^{\mathcal{NN}} \left(\frac{\cosh(i\bar{\eta}'_n y)}{\cosh(i\bar{\eta}'_n b_1)} \right) \cos(-\pi n).$$

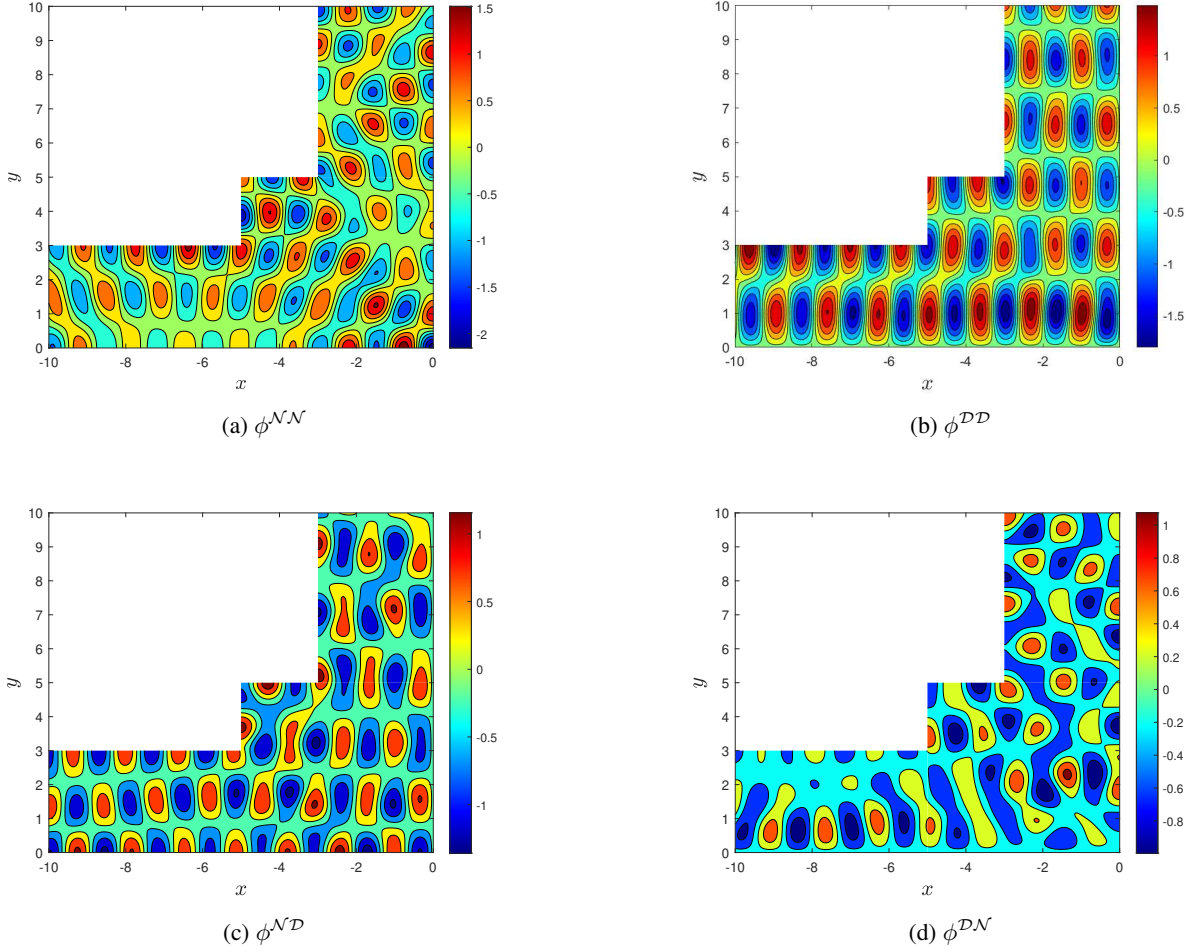


Figure 4: Contour plots of the real parts of (a) $\phi^{\mathcal{NN}}$, (b) $\phi^{\mathcal{DD}}$, (c) $\phi^{\mathcal{ND}}$, and (d) $\phi^{\mathcal{DN}}$ for the cases where $a_1 = a_2 = 3$, $b_1 = b_2 = 5$, $k = 5$, and $N = 100$. The incident mode is $p = 2$ in panels (a) and (c), and $p = 1$ in panels (b) and (d). Note that contour lines being parallel or perpendicular to a boundary indicate homogeneous Dirichlet or Neumann boundary conditions, respectively.

for $p = 0$, and by

$$\left(\frac{2\bar{\beta}_0}{\bar{\beta}_p}\right) (|A_0^{\mathcal{NN}}|^2 + |D_0^{\mathcal{NN}}|^2) + \sum_{n=1}^q \left(\frac{\bar{\beta}_n}{\bar{\beta}_p}\right) (|A_n^{\mathcal{NN}}|^2 + |D_n^{\mathcal{NN}}|^2) = 1, \quad (45b)$$

for $p \neq 0$ where $q = \lfloor \frac{ka_1}{\pi} \rfloor$ is the number of even propagating modes.

4 The Scattering Matrix

Here, we outline a scattering matrix for the four-waveguide problem, which could be used to extend our methods to multiple scattering problems, such as the one illustrated in Figure 1. For simplicity, we only consider the case $a_1 = a_2$ and $b_1 = b_2$, although our discussion can be extended to the more general case. The scattering matrix satisfies

$$\mathcal{S}\mathbf{a} = \mathbf{b}, \quad (46)$$

where the entries of \mathbf{a} are the coefficients of the incident wave entering the channels, and the entries of \mathbf{b} are the coefficients of the outgoing waves. We express these vectors as

$$\mathbf{a} = \begin{bmatrix} \mathbf{a}_{\text{even},\rightarrow} \\ \mathbf{a}_{\text{odd},\rightarrow} \\ \mathbf{a}_{\text{even},\downarrow} \\ \mathbf{a}_{\text{odd},\downarrow} \\ \mathbf{a}_{\text{even},\leftarrow} \\ \mathbf{a}_{\text{odd},\leftarrow} \\ \mathbf{a}_{\text{even},\uparrow} \\ \mathbf{a}_{\text{odd},\uparrow} \end{bmatrix}, \quad \text{and} \quad \mathbf{b} = \begin{bmatrix} \mathbf{b}_{\text{even},\leftarrow} \\ \mathbf{b}_{\text{odd},\leftarrow} \\ \mathbf{b}_{\text{even},\uparrow} \\ \mathbf{b}_{\text{odd},\uparrow} \\ \mathbf{b}_{\text{even},\rightarrow} \\ \mathbf{b}_{\text{odd},\rightarrow} \\ \mathbf{b}_{\text{even},\downarrow} \\ \mathbf{b}_{\text{odd},\downarrow} \end{bmatrix}$$

where $\mathbf{a}_{\text{even},\rightarrow}$, $\mathbf{a}_{\text{even},\downarrow}$, $\mathbf{a}_{\text{even},\leftarrow}$ and $\mathbf{a}_{\text{even},\uparrow}$ denote the amplitude coefficients of even incident waves entering from the left, top, right and bottom channels, respectively, whereas $\mathbf{b}_{\text{even},\leftarrow}$, $\mathbf{b}_{\text{even},\uparrow}$, $\mathbf{b}_{\text{even},\rightarrow}$ and $\mathbf{b}_{\text{even},\downarrow}$ denote the amplitude coefficients of even outgoing waves exiting through the left, top, right and bottom channels, respectively. The remaining subvectors of \mathbf{a} and \mathbf{b} , which correspond to waves with odd symmetry, are defined similarly. We assume that the wide spacing approximation will be applied to the ensuing multiple scattering problem, so evanescent incident/outgoing wave components are not considered. Thus, the vectors of even wave coefficients are of length $q + 1$, where we recall $q = \lfloor \frac{ka_1}{\pi} \rfloor$, and the vectors of odd wave coefficients are of length $\tilde{q} = \lfloor \frac{2ka_1 - \pi}{2\pi} \rfloor$, being the number of odd propagating modes. The scattering matrix \mathcal{S} is expressed as an 8×8 block matrix of the form

$$\mathcal{S} = \begin{bmatrix} S_{\text{even},\rightarrow}^{\text{even},\leftarrow} & [0] & S_{\text{even},\rightarrow}^{\text{even},\downarrow} & S_{\text{even},\rightarrow}^{\text{even},\leftarrow} & S_{\text{even},\rightarrow}^{\text{even},\leftarrow} & [0] & S_{\text{even},\rightarrow}^{\text{even},\uparrow} & S_{\text{even},\rightarrow}^{\text{even},\leftarrow} \\ [0] & S_{\text{odd},\rightarrow}^{\text{odd},\leftarrow} & S_{\text{odd},\rightarrow}^{\text{odd},\downarrow} & S_{\text{odd},\rightarrow}^{\text{odd},\leftarrow} & [0] & S_{\text{odd},\rightarrow}^{\text{odd},\leftarrow} & S_{\text{odd},\rightarrow}^{\text{odd},\uparrow} & S_{\text{odd},\rightarrow}^{\text{odd},\leftarrow} \\ S_{\text{even},\rightarrow}^{\text{even},\uparrow} & S_{\text{even},\rightarrow}^{\text{even},\uparrow} & S_{\text{even},\rightarrow}^{\text{even},\downarrow} & [0] & S_{\text{even},\rightarrow}^{\text{even},\leftarrow} & S_{\text{even},\rightarrow}^{\text{even},\uparrow} & S_{\text{even},\rightarrow}^{\text{even},\uparrow} & [0] \\ S_{\text{odd},\rightarrow}^{\text{odd},\uparrow} & S_{\text{odd},\rightarrow}^{\text{odd},\uparrow} & [0] & S_{\text{odd},\rightarrow}^{\text{odd},\uparrow} & S_{\text{even},\rightarrow}^{\text{even},\leftarrow} & S_{\text{odd},\rightarrow}^{\text{odd},\uparrow} & S_{\text{odd},\rightarrow}^{\text{odd},\uparrow} & S_{\text{odd},\rightarrow}^{\text{odd},\uparrow} \\ S_{\text{even},\rightarrow}^{\text{even},\rightarrow} & [0] & S_{\text{even},\rightarrow}^{\text{even},\downarrow} & S_{\text{odd},\rightarrow}^{\text{odd},\downarrow} & S_{\text{even},\rightarrow}^{\text{even},\leftarrow} & [0] & S_{\text{even},\rightarrow}^{\text{even},\uparrow} & S_{\text{odd},\rightarrow}^{\text{odd},\downarrow} \\ [0] & S_{\text{odd},\rightarrow}^{\text{odd},\rightarrow} & S_{\text{odd},\rightarrow}^{\text{odd},\downarrow} & S_{\text{odd},\rightarrow}^{\text{odd},\downarrow} & [0] & S_{\text{odd},\rightarrow}^{\text{odd},\rightarrow} & S_{\text{odd},\rightarrow}^{\text{odd},\uparrow} & S_{\text{odd},\rightarrow}^{\text{odd},\downarrow} \\ S_{\text{even},\rightarrow}^{\text{even},\downarrow} & S_{\text{even},\rightarrow}^{\text{even},\downarrow} & S_{\text{even},\rightarrow}^{\text{even},\downarrow} & [0] & S_{\text{even},\rightarrow}^{\text{even},\downarrow} & S_{\text{even},\rightarrow}^{\text{even},\downarrow} & S_{\text{even},\rightarrow}^{\text{even},\downarrow} & [0] \\ S_{\text{odd},\rightarrow}^{\text{odd},\downarrow} & S_{\text{odd},\rightarrow}^{\text{odd},\downarrow} & [0] & S_{\text{odd},\rightarrow}^{\text{odd},\downarrow} & S_{\text{odd},\rightarrow}^{\text{odd},\downarrow} & S_{\text{odd},\rightarrow}^{\text{odd},\downarrow} & [0] & S_{\text{odd},\rightarrow}^{\text{odd},\downarrow} \end{bmatrix}.$$

where the notation of the submatrices is defined so that, for example, $S_{\text{even},\rightarrow}^{\text{odd},\uparrow}$ gives the coefficients of odd outgoing waves travelling upwards towards $y = +\infty$ due to excitation by even incident waves travelling right from $x = -\infty$. The scattering matrix contains zero matrices $[0]$ due to symmetry restrictions, as for example, a wave of even symmetry incident from $x = -\infty$ cannot excite waves of odd symmetry outgoing towards $x = \pm\infty$.

In the case where $k = 4$ and $a_1 = a_2 = 2$, there are three propagating symmetric modes and two propagating antisymmetric modes in each channel. This means that vectors of the form \mathbf{a}_{even} and \mathbf{b}_{even} are of length $q+1=3$, while vectors of the form \mathbf{a}_{odd} and \mathbf{b}_{odd} are of length $\tilde{q} = 2$. The entries of the nonzero submatrices of \mathcal{S} can be computed from our solution. For brevity, only two examples are given here. The matrix $S_{\text{even},\rightarrow}^{\text{even},\leftarrow}$ is of dimension 3×3 . Its first column is $\frac{1}{2}[A_0^{\mathcal{N}\mathcal{N}} + A_0^{\mathcal{D}\mathcal{N}}, A_1^{\mathcal{N}\mathcal{N}} + A_1^{\mathcal{D}\mathcal{N}}, A_2^{\mathcal{N}\mathcal{N}} + A_2^{\mathcal{D}\mathcal{N}}]^T$, in which the coefficients $A_m^{\mathcal{N}\mathcal{N}}$ and $A_m^{\mathcal{D}\mathcal{N}}$ are computed for the case when the incident wave mode is $p = 0$. The second and third columns are also of this form, but computed for the cases when $p = 1$ and $p = 2$, respectively. The matrix $S_{\text{odd},\rightarrow}^{\text{odd},\leftarrow}$ is of the dimension 2×2 . Its first column is $\frac{1}{2}[A_1^{\mathcal{D}\mathcal{D}} + A_1^{\mathcal{N}\mathcal{D}}, A_2^{\mathcal{D}\mathcal{D}} + A_2^{\mathcal{N}\mathcal{D}}]^T$, in which the coefficients $A_m^{\mathcal{D}\mathcal{D}}$ and $A_m^{\mathcal{N}\mathcal{D}}$ are computed for the case when the incident wave mode is $p = 1$. The second column is of the same form, but calculated for the case when $p = 2$.

5 Time-domain results

A time-domain solution is given as a continuous superposition of frequency domain solutions, as described in Eq. (4). After approximating the continuous superposition using a quadrature rule, the computation of the time domain solution reduces to matrix multiplication [39, 40, 41]. To do this, the integral over k in (4) is approximated using the quadrature rule of the form

$$\int_0^\infty g(k)dk \approx \sum_{j=1}^{N_k} g(k_j)w_j, \quad (47)$$

where $k_j = j\Delta k$ are the quadrature points and w_i are the quadrature weights. In the case of the trapezoidal rule, these weights are

$$w_j = \begin{cases} \Delta k/2, & \text{if } j = 1 \text{ or } j = N_k, \\ \Delta k, & \text{otherwise.} \end{cases}$$

After applying this quadrature rule, (4) becomes

$$\varphi(x, y, t) \approx \operatorname{Re} \left\{ \sum_{j=1}^{N_k} \hat{f}(k_j) \phi(x, y, k_j) e^{-ik_j t} w_j \right\}. \quad (48)$$

Note that the general time domain solution is a superposition over incident modes p and over all four incident directions, but for simplicity we restrict to the case where the incident mode p is fixed and the wave is incident from $x = -\infty$. Next, we let (x_i, y_i) for $1 \leq i \leq N_x$ be the points at which we want to evaluate our time domain solution. Equation (48) can then be represented using matrix multiplication as

$$\varphi(t) \approx \operatorname{Re} \left\{ [\phi] \operatorname{Diag}(w_j e^{-ik_j t}) \hat{\mathbf{f}} \right\}$$

where we have defined $\varphi(t)$ to be the vector of length N_x with entries $\varphi(x_i, y_i, t)$ and $[\phi]$ to be the matrix with entries $[\phi]_{ij} = \phi(x_i, y_i, k_j)$. Moreover, $\hat{\mathbf{f}}$ is the vector of length N_k with entries $\hat{f}(k_j)$. Note that the calculation of the frequency domain solution matrix $[\phi]$ is the main computational expense of our time domain solution. In this formulation, this calculation only needs to be done once for a particular set of parameters, so that the solutions for different amplitude spectra \hat{f} can be computed quickly.

Figures 5–8 show time domain solutions for a range of different parameters and incident spectra \hat{f} . In each figure, the panels show snapshots from Movies 1–4 at a range of different times, which illustrate the scattering of an incident wave travelling from left to right. The special cases $a_1 = b_1$ and $a_2 = b_2$, in which the dimensions of the rectangular region match those of the waveguides, are shown in Figures 6 and 8. Figure 7 shows the case where the incident wave is of odd symmetry about $y = 0$, with the remaining figures showing cases of even incident waves. Note that all Movies are provided in the supplementary material.

6 Conclusions

In this investigation, we applied a symmetry-based decomposition and the eigenfunction matching technique to solve the problem of wave scattering at a rectangular junction of four waveguides in the frequency domain. Subsequently, the time-domain solution was obtained as a continuous superposition of frequency domain solutions, and results were given for a range of incident pulses and waveguide geometries. Additionally, we described how to use our solution to obtain the scattering matrix for the junction. Future work could use this scattering matrix to solve the problem of wave propagation through a square lattice of such junctions, thereby forming a connection with the subresonant lattices studied in quantum graph theory [38, 37]

A Eigenfunction matching of the remaining cases

We determine the matching conditions of both discontinuities in the case of Dirichlet-Dirichlet problem. On using (26), (28) and (29) into the matching condition (13a) to obtain

$$\begin{aligned} \tilde{\Phi}_p(y) + \sum_{n=0}^{\infty} A_n^{\mathcal{D}\mathcal{D}} \tilde{\Phi}_n(y) &= \sum_{n=0}^{\infty} B_n^{\mathcal{D}\mathcal{D}} \tilde{\Gamma}_n(y) \\ &+ \sum_{n=0}^{\infty} C_n^{\mathcal{D}\mathcal{D}} \left(\frac{\sinh(i\bar{\zeta}_n y)}{\sinh(i\bar{\zeta}_n b_1)} \right) \sin \left((-2n+1) \frac{\pi}{2} \right). \end{aligned} \quad (49)$$

Taking the inner product with $\bar{\Phi}_m(y)$ and integrating over $[0, a_1]$, then using Eq. (27), yields

$$\hat{I}_{mp}(a_1) + A_m^{\mathcal{D}\mathcal{D}} \hat{I}_{mn}(a_1) = \sum_{n=0}^{\infty} B_n^{\mathcal{D}\mathcal{D}} R_{mn} + \sum_{n=0}^{\infty} C_n^{\mathcal{D}\mathcal{D}} Q_{mn}, \quad m = 0, 1, 2, \dots, \quad (50)$$

where R_{mn} and Q_{mn} are stated in 69 and 70. On using (30), (28) and (29) into (13b) to derive the matching at $y = b_1$ as

$$\sum_{n=0}^{\infty} D_n^{\mathcal{D}\mathcal{D}} \tilde{\aleph}_n(x) = \sum_{n=0}^{\infty} B_n^{\mathcal{D}\mathcal{D}} \left(\frac{\sinh(i\bar{\lambda}_n x)}{\sinh(-i\bar{\lambda}_n b_2)} \right) \sin((2n+1)\pi/2) + \sum_{n=0}^{\infty} C_n^{\mathcal{D}\mathcal{D}} \tilde{\Upsilon}_n(x), \quad (51)$$

we take the inner product with $\bar{\Omega}_m(x)$, and integrate over $[-a_2, 0]$, yields

$$D_m^{\mathcal{D}\mathcal{D}} \hat{I}_{mn}(a_2) = \sum_{n=0}^{\infty} B_n^{\mathcal{D}\mathcal{D}} W_{mn} + \sum_{n=0}^{\infty} C_n^{\mathcal{D}\mathcal{D}} K_{mn}, \quad m = 0, 1, 2, \dots, \quad (52)$$

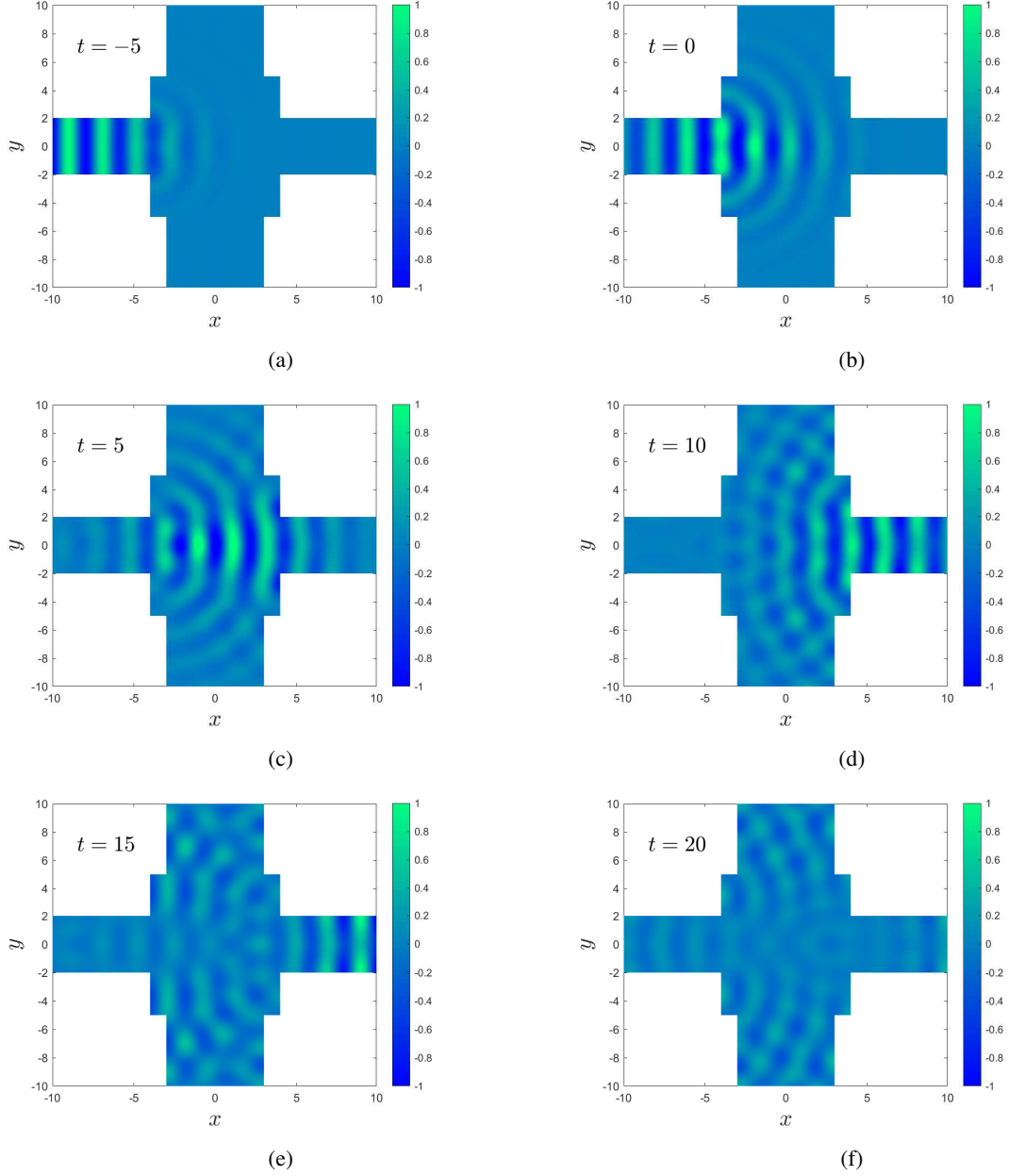


Figure 5: Snapshots showing the scattering of a symmetric incident wave at times (a) $t = -5$, (b) $t = 0$, (c) $t = 5$, (d) $t = 10$, (e) $t = 15$, and (f) $t = 20$. The parameters used are $p = 0$, $b_1 = 5$, $b_2 = 4$, $a_1 = 2$, $a_2 = 3$, $k = 10$, and $N = 100$. The incident spectrum was chosen to be $\hat{f}(k) = \frac{1}{\pi} e^{-8(k-3)^2}$.

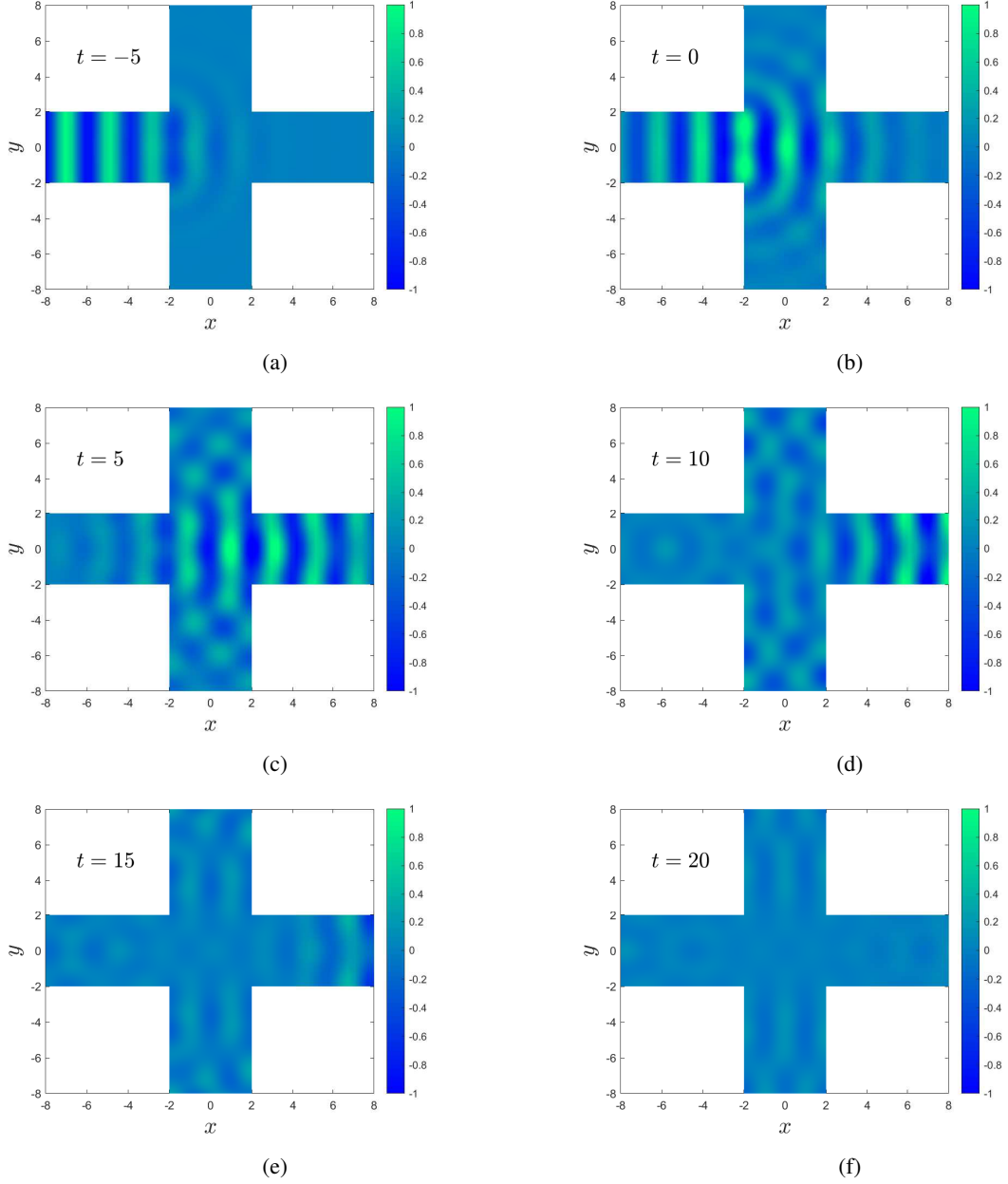


Figure 6: Snapshots showing the scattering of a symmetric incident wave at times (a) $t = -5$, (b) $t = 0$, (c) $t = 5$, (d) $t = 10$, (e) $t = 15$, and (f) $t = 20$. The parameters used are $p = 0$, $N = 100$, $k = 15$, and $a_1 = a_2 = b_1 = b_2 = 2$. The incident spectrum was chosen to be $\hat{f}(k) = \frac{1}{\pi}e^{-8(k-3)^2}$.

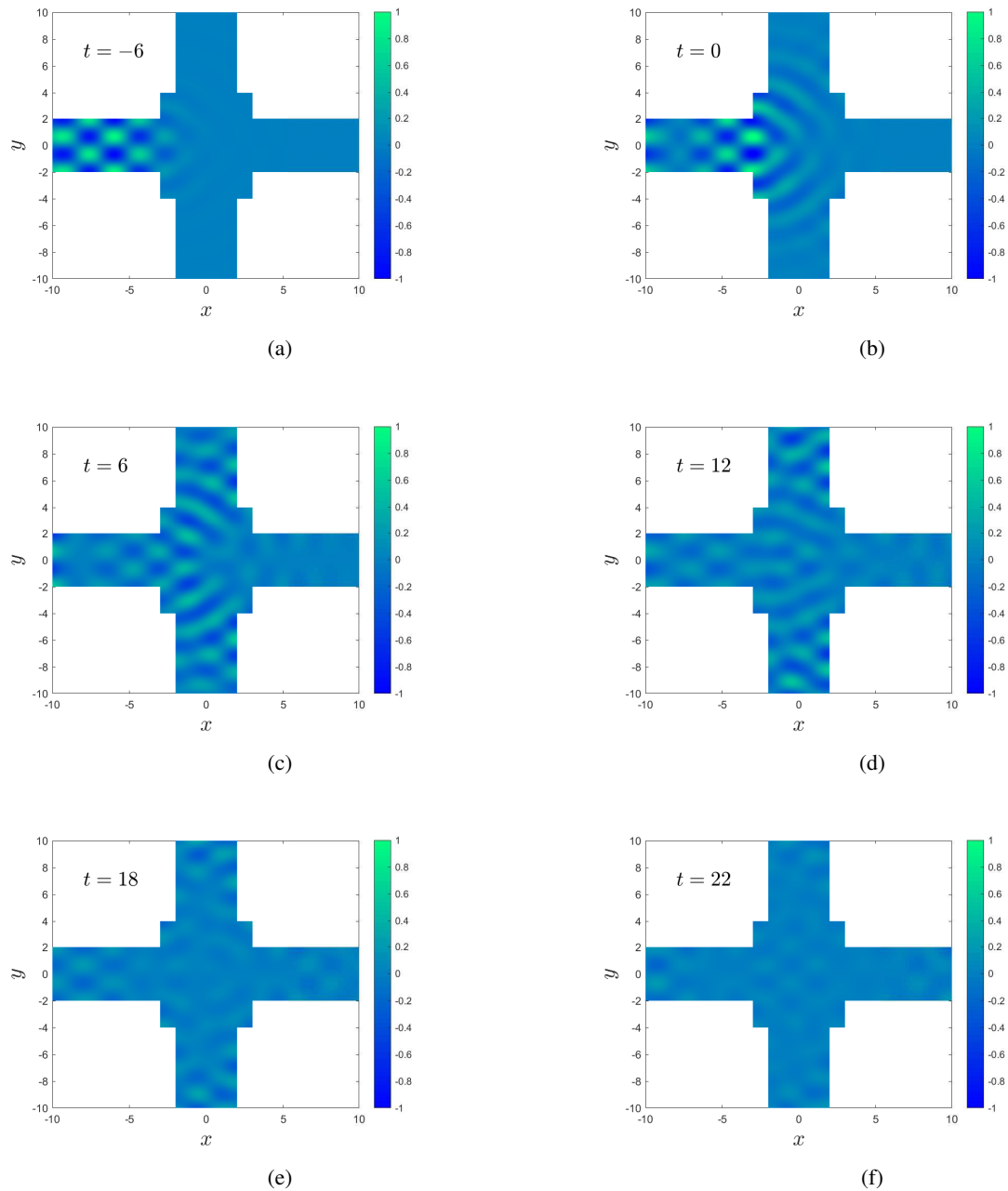


Figure 7: Snapshots showing the scattering of an antisymmetric incident wave at times: (a) $t = -6$, (b) $t = 0$, (c) $t = 6$, (d) $t = 12$, (e) $t = 18$, and (f) $t = 22$. The parameters used are $p = 1$, $b_1 = 4$, $b_2 = 3$, $a_1 = a_2 = 2$, $k = 12$, and $N = 100$. The incident spectrum is $\hat{f}(k) = \frac{1}{\pi} e^{-9(k-3)^2}$.

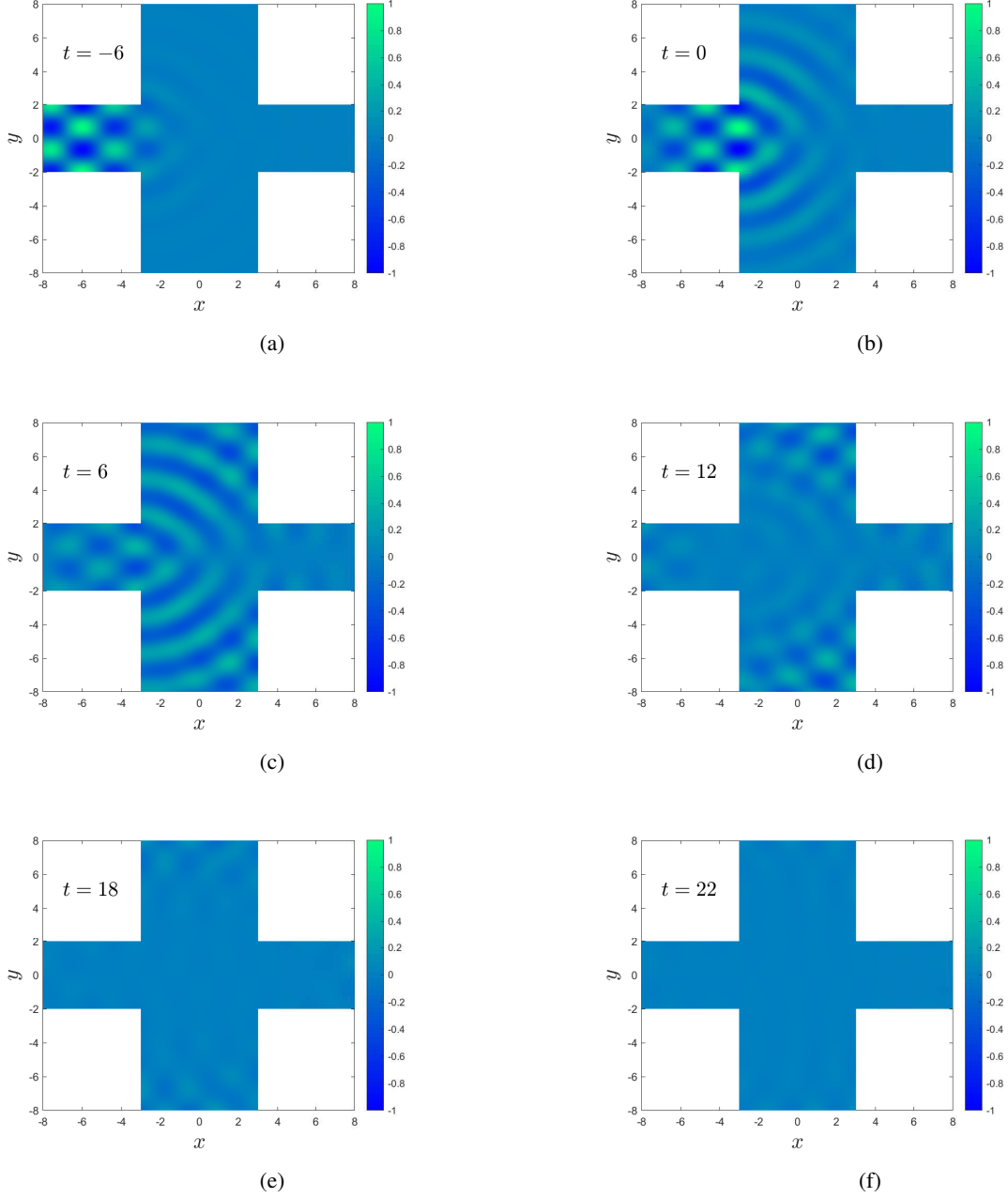


Figure 8: Showing the scattering of an antisymmetric incident wave at times: (a) $t = -6$, (b) $t = 0$, (c) $t = 6$, (d) $t = 12$, (e) $t = 18$, and (f) $t = 22$. The parameters used are $p = 1$, $b_1 = 4$, $b_2 = a_2 = 3$, a_2 , $k = 8$, and $N = 100$. The incident spectrum was chosen as $\hat{f}(k) = \frac{1}{\pi}e^{-9(k-3)^2}$.

where W_{mn} and K_{mn} are stated in 71 and 72. In addition, on using the derivative of (26), (28) and (29) with respect to x into the matching condition (14a) to obtain

$$\bar{\gamma}_p \tilde{\Phi}_p(y) - \sum_{n=0}^{\infty} A_n^{\mathcal{D}\mathcal{D}} \bar{\gamma}_n \tilde{\Phi}_n(y) = \sum_{n=0}^{\infty} B_n^{\mathcal{D}\mathcal{D}} \bar{\lambda}_n \coth(-i\bar{\lambda}_n b_2) \tilde{\Gamma}_n(y). \quad (53)$$

Taking the inner product with $\tilde{\Gamma}_n(y)$, and integrate over $[0, b_1]$ and then using Eq. (69), yields

$$\bar{\gamma}_p R_{pm} - \sum_{n=0}^{\infty} A_n^{\mathcal{D}\mathcal{D}} \bar{\gamma}_n R_{nm} = B_m^{\mathcal{D}\mathcal{D}} \bar{\lambda}_m \coth(-i\bar{\lambda}_m b_2) \hat{I}_{mn}(b_1), \quad m = 0, 1, 2, \dots \quad (54)$$

On using the derivative of (30), (28) and (29) with respect to y into (14b) to obtain

$$\sum_{n=0}^{\infty} D_n^{\mathcal{D}\mathcal{D}} \bar{\zeta}'_n \tilde{\aleph}_n(x) = \sum_{n=0}^{\infty} C_n^{\mathcal{D}\mathcal{D}} \bar{\zeta}_n \coth(i\bar{\zeta}_n b_1) \tilde{\Upsilon}_n(x). \quad (55)$$

Taking the inner product with $\tilde{\Upsilon}_m(y)$ and integrate over $[-b_2, 0]$ and then using (72), yields

$$\sum_{n=0}^{\infty} D_n^{\mathcal{D}\mathcal{D}} \bar{\zeta}'_n K_{nm} = C_m^{\mathcal{D}\mathcal{D}} \bar{\zeta}_m \coth(i\bar{\zeta}_m b_1) \hat{I}_{mn}(b_2), \quad m = 0, 1, 2, \dots \quad (56)$$

We proceeded with an almost identical method to the previous two cases to obtain the matching conditions in the Neumann-Dirichlet problem. We used (26), (33) and (34) and then (22), (33) and (34) are matched using (13a) and (13b) respectively. Then, using (27), (69), (68) to obtain the expressions

$$\hat{I}_{mp}(a_1) + A_m^{\mathcal{N}\mathcal{D}} \hat{I}_{mn}(a_1) = \sum_{n=0}^{\infty} B_n^{\mathcal{N}\mathcal{D}} R_{mn} + \sum_{n=0}^{\infty} C_n^{\mathcal{N}\mathcal{D}} V'_{mn}, \quad m = 0, 1, 2, \dots, \quad (57)$$

$$D_m^{\mathcal{N}\mathcal{D}} I_{mn}(a_1) = \sum_{n=0}^{\infty} B_n^{\mathcal{N}\mathcal{D}} W'_{mn} + \sum_{n=0}^{\infty} C_n^{\mathcal{N}\mathcal{D}} E_{mn}, \quad m = 0, 1, 2, \dots, \quad (58)$$

where V'_{mn} and W'_{mn} are given in 73 and 74. The derivative of (26), (33) and (34) and then (22), (33) and (34) with respect to x and then y are matched using (14a) and (14b) respectively. Simplifying by using (69) and (68) to obtain

$$\bar{\gamma}_p R_{pm} - \sum_{n=0}^{\infty} A_n^{\mathcal{N}\mathcal{D}} \bar{\gamma}_n R_{nm} = B_m^{\mathcal{N}\mathcal{D}} \bar{\lambda}_m \tanh(-i\bar{\lambda}_m b_2) \hat{I}_{mn}(b_1), \quad m = 0, 1, 2, \dots, \quad (59)$$

$$\sum_{n=0}^{\infty} D_n^{\mathcal{N}\mathcal{D}} \bar{\eta}'_n E_{nm} = C_m^{\mathcal{N}\mathcal{D}} \bar{\eta}'_m \coth(i\bar{\eta}'_m b_1) I_{mn}(b_2), \quad m = 0, 1, 2, \dots, \quad (60)$$

Now, we derive the matching conditions in the Dirichlet-Neumann problem and follow a nearly identical process. We match (18), (37) and (38) into (13a) and then (30), (37) and (38) into (13b). Using (65) and (72) to obtain

$$I_{mp}(a_1) + A_m^{\mathcal{D}\mathcal{N}} I_{mn}(a_1) = \sum_{n=0}^{\infty} B_n^{\mathcal{D}\mathcal{N}} H_{mn} + \sum_{n=0}^{\infty} C_n^{\mathcal{D}\mathcal{N}} Q'_{mn}, \quad m = 0, 1, 2, \dots, \quad (61)$$

$$D_m^{\mathcal{D}\mathcal{N}} \hat{I}_{mn}(a_2) = \sum_{n=0}^{\infty} B_n^{\mathcal{D}\mathcal{N}} O'_{mn} + \sum_{n=0}^{\infty} C_n^{\mathcal{D}\mathcal{N}} K_{mn}, \quad m = 0, 1, 2, \dots, \quad (62)$$

where Q'_{mn} and O'_{mn} are given in 75 and 76. Then, we substitute the derivative of (18), (37) and (38) into (14a) and then (30), (37) and (38) into (14b) with respect to x and then y . Using (65) and (72) to obtain

$$\bar{\beta}_p H_{pm} - \sum_{n=0}^{\infty} A_n^{\mathcal{D}\mathcal{N}} \bar{\beta}_n H_{nm} = B_m^{\mathcal{D}\mathcal{N}} \bar{\alpha}_m \coth(-i\bar{\alpha}_m b_2) I_{mn}(b_1), \quad (63)$$

$$\sum_{n=0}^{\infty} D_n^{\mathcal{D}\mathcal{N}} \bar{\zeta}'_n K_{nm} = C_m^{\mathcal{D}\mathcal{N}} \bar{\zeta}_m \tanh(i\bar{\zeta}_m b_1) \hat{I}_{mn}(a_2). \quad (64)$$

To solve these systems numerically, we express the system of equations (50), (52), (54) and (56) as

$$\begin{bmatrix} [-\text{diag}(\hat{I}_{mn}(a_1))] & [R_{mn}] & [Q_{mn}] & [0] \\ [0] & [W_{mn}] & [K_{mn}] & [-\text{diag}(\hat{I}_{mn}(a_2))] \\ [\text{diag}(\tilde{\gamma}_n)R_{mn}^T] & [\text{diag}(\bar{\lambda}_m \coth(-i\bar{\lambda}_m b_2)\hat{I}_{mn}(b_1))] & [0] & [0] \\ [0] & [0] & [\text{diag}(\bar{\zeta}_m \coth(i\bar{\zeta}_m b_1)\hat{I}_{mn}(b_2))] & [-\text{diag}(\bar{\zeta}'_n)K_{mn}^T] \end{bmatrix} \begin{bmatrix} [A_n^{\mathcal{D}\mathcal{D}}] \\ [B_n^{\mathcal{D}\mathcal{D}}] \\ [C_n^{\mathcal{D}\mathcal{D}}] \\ [D_n^{\mathcal{D}\mathcal{D}}] \end{bmatrix} = \begin{bmatrix} [\hat{I}_{mn}(a_1)] \\ [0] \\ [\tilde{\gamma}_n R_{pm}^T] \\ [0] \end{bmatrix}.$$

Additionally, we express (57), (58), (59) and (60) as

$$\begin{bmatrix} [-\text{diag}(\hat{I}_{mn}(a_1))] & [R_{mn}] & [V'_{mn}] & [0] \\ [0] & [W'_{mn}] & [E_{mn}] & [-\text{diag}(\hat{I}_{mn}(a_2))] \\ [\text{diag}(\tilde{\gamma}_n)R_{mn}^T] & [\text{diag}(\bar{\lambda}_m \tanh(-i\bar{\lambda}_m b_2)\hat{I}_{mn}(b_1))] & [0] & [0] \\ [0] & [0] & [\text{diag}(\bar{\eta}'_m \coth(i\bar{\eta}'_m b_1)\hat{I}_{mn}(b_2))] & [-\text{diag}(\bar{\eta}_n)E_{mn}^T] \end{bmatrix} \begin{bmatrix} [A_n^{\mathcal{N}\mathcal{D}}] \\ [B_n^{\mathcal{N}\mathcal{D}}] \\ [C_n^{\mathcal{N}\mathcal{D}}] \\ [D_n^{\mathcal{N}\mathcal{D}}] \end{bmatrix} = \begin{bmatrix} [\hat{I}_{mn}(a_1)] \\ [0] \\ [\tilde{\gamma}_n R_{pm}^T] \\ [0] \end{bmatrix}.$$

Then, we express (61), (62), (63) and (64) as

$$\begin{bmatrix} [-\text{diag}(I_{mn}(a_1))] & [H_{mn}] & [Q'_{mn}] & [0] \\ [0] & [O'_{mn}] & [K_{mn}] & [-\text{diag}(\hat{I}_{mn}(a_2))] \\ [\text{diag}(\bar{\beta}_n)H_{mn}^T] & [\text{diag}(\bar{\alpha}_m \coth(-i\bar{\alpha}_m b_2)I_{mn}(b_1))] & [0] & [0] \\ [0] & [0] & [\text{diag}(\bar{\zeta}_m \tanh(i\bar{\zeta}_m b_1)\hat{I}_{mn}(b_2))] & [-\text{diag}(\bar{\zeta}'_n)K_{mn}^T] \end{bmatrix} \begin{bmatrix} [A_n^{\mathcal{D}\mathcal{N}}] \\ [B_n^{\mathcal{D}\mathcal{N}}] \\ [C_n^{\mathcal{D}\mathcal{N}}] \\ [D_n^{\mathcal{D}\mathcal{N}}] \end{bmatrix} = \begin{bmatrix} [I_{mn}(a_1)] \\ [0] \\ [\bar{\beta}_n H_{pm}^T] \\ [0] \end{bmatrix}.$$

Where the outer bracket denotes the matrix.

B The matrix elements calculations

We explore the integrations that have been used to solve the four matrices, respectively

$$\begin{aligned}
H_{mn} &= \int_0^{a_1} \Gamma_n(y) \Phi_m(y) dy & (65) \\
&= \begin{cases} a_1, & \text{if } \beta_m = \alpha_n = 0, \\ a_1/2 + \sin(2a_1\beta_m)/(4\beta_m), & \text{if } \beta_m = \alpha_n \neq 0, \\ \sin(a_1(\alpha_n + \beta_m))/(2(\alpha_n + \beta_m)) \\ + \sin(a_1(\alpha_n - \beta_m))/(2(\alpha_n - \beta_m)), & \text{if } \beta_m \neq \alpha_n. \end{cases}
\end{aligned}$$

$$\begin{aligned}
V_{mn} &= \int_0^{a_1} \left(\cosh(i\bar{\eta}'_n y) / \cosh(i\bar{\eta}'_n b_1) \right) \cos(-n\pi) \Phi_m(y) dy & (66) \\
&= \begin{cases} a_1 / \cosh(i\bar{\eta}'_n b_1) \cos(-n\pi), & \text{if } \beta_m = \bar{\eta}'_n = 0, \\ \sin(a_1\beta_m(1-1i))(1+1i) + \sin(a_1\beta_m(1+1i)) \\ (1-1i)/(4\beta_m) / \cosh(i\bar{\eta}'_n b_1) \cos(-n\pi), & \text{if } \beta_m = \bar{\eta}'_n \neq 0, \\ (\beta_m \cos(a_1\eta_n) \sin(a_1\beta_m) - \bar{\eta}'_n \cos(a_1\beta_m) \sin(a_1\bar{\eta}'_n)) \\ / (\beta_m^2 - \bar{\eta}'_n{}^2) / \cosh(i\bar{\eta}'_n b_1) \cos(-n\pi), & \text{if } \beta_m \neq \bar{\eta}'_n. \end{cases}
\end{aligned}$$

$$\begin{aligned}
O_{mn} &= \int_{-a_2}^0 \left(\cosh(i\bar{\alpha}_n x) / \cosh(-i\bar{\alpha}_n b_2) \right) \cos(n\pi) \Omega_m(x) dx & (67) \\
&= \begin{cases} a_2 / \cosh(-i\bar{\alpha}_n b_2) \cos(n\pi), & \text{if } i\bar{\alpha}_n = \eta_m = 0, \\ (\sin(a_2\eta_m(1-1i))(1+1i) + \sin(a_2\eta_m(1+1i)) \\ (1-1i)/(4\eta_m) / \cosh(-i\bar{\alpha}_n b_2) \cos(n\pi), & \text{if } i\bar{\alpha}_n = \eta_m \neq 0, \\ (\eta_m \cos(a_2\alpha_n) \sin(a_2\eta_m) - \alpha_n \cos(a_2\eta_m) \sin(a_2\alpha_n)) \\ / (\eta_m^2 - \alpha_n^2) / \cosh(-i\bar{\alpha}_n b_2) \cos(n\pi), & \text{if } i\bar{\alpha}_n \neq \eta_m. \end{cases}
\end{aligned}$$

$$\begin{aligned}
E_{mn} &= \int_{-a_2}^0 \Upsilon_n(x) \Omega_m(x) dx & (68) \\
&= \begin{cases} a_2, & \text{if } \eta'_n = \eta_m = 0, \\ a_2/2 + \sin(2a_2\eta_m)/(4\eta_m), & \text{if } \eta'_n = \eta_m \neq 0, \\ \sin(a_2(\eta_m - \eta'_n))/(2(\eta_m - \eta'_n)) + \sin(a_2(\eta_m + \eta'_n)) \\ / (2(\eta_m + \eta'_n)), & \text{if } \eta'_n \neq \eta_m. \end{cases}
\end{aligned}$$

$$\begin{aligned}
R_{mn} &= \int_0^{a_1} \bar{\Gamma}_n(y) \bar{\Phi}_m(y) dy & (69) \\
&= \begin{cases} a_1/2 - \sin(2a_1\gamma_m)/(4\gamma_m), & \text{if } \gamma_m = \lambda_n, \\ -(\gamma_m \cos(a_1\gamma_m) \sin(a_1\lambda_n) - \lambda_n \cos(a_1\lambda_n) \\ \sin(a_1\gamma_m)/(\gamma_m^2 - \lambda_n^2), & \text{if } \gamma_m \neq \lambda_n. \end{cases}
\end{aligned}$$

$$\begin{aligned}
Q_{mn} &= \int_0^{a_1} \left(\sinh(i\bar{\zeta}_n y) / \sinh(i\bar{\zeta}_n b_1) \right) \sin(-(2n+1)\pi/2) \bar{\Phi}_m(y) dy & (70) \\
&= \begin{cases} -(\cos(a_1\gamma_m) \sinh(a_1\gamma_m) - \cosh(a_1\gamma_m) \sin(a_1\gamma_m)) \\ / (2\gamma_m) \sinh(i\bar{\zeta}_n b_1) \sin(-(2n+1)\pi/2), & \text{if } \gamma_m = i\bar{\zeta}_n, \\ -i(\gamma_m \cos(a_1\gamma_m) \sin(a_1\bar{\zeta}_n) i - \bar{\zeta}_n \sin(a_1\gamma_m) \\ \cos(a_1\bar{\zeta}_n) i) / (\gamma_m^2 - \bar{\zeta}_n^2) \sinh(i\bar{\zeta}_n b_1) \sin(-(2n+1)\pi/2), & \text{if } \gamma_m \neq i\bar{\zeta}_n. \end{cases}
\end{aligned}$$

$$\begin{aligned}
W_{mn} &= \int_{-a_2}^0 (\sinh(i\bar{\lambda}_n x) / \sinh(-i\bar{\lambda}_n b_2)) \sin((2n+1)\pi/2) \bar{\Omega}_m(x) dx \\
&= \begin{cases} -(\cos(a_2 \zeta_m) \sinh(a_2 \zeta_m) - \cosh(a_2 \zeta_m) \sin(a_2 \zeta_m)) / (2\zeta_m) \\ \sinh(-i\bar{\lambda}_n(b_2)) \sin((2n+1)\pi/2), & \text{if } i\bar{\lambda} = \zeta'_m \neq 0, \\ -(\bar{\lambda}_n \cos(a_2 \bar{\lambda}_n) \sin(a_2 \zeta_m) i - \zeta_m \cos(a_2 \zeta_m) \sin(a_2 \bar{\lambda}_n) i) \\ / (\bar{\lambda}_n^2 - \zeta_m^2) \sinh(-i\bar{\lambda}_n(b_2)) \sin((2n+1)\pi/2), & \text{if } i\bar{\lambda} \neq \zeta'_m. \end{cases}
\end{aligned} \tag{71}$$

$$\begin{aligned}
K_{mn} &= \int_{-a_2}^0 \bar{\Upsilon}_n(x) \bar{\Omega}_m(x) dx \\
&= \begin{cases} a_2/2, & \text{if } \zeta_n = \zeta'_m, \\ -(\zeta'_m \cos(a_2 \zeta'_m) \sin(a_2 \zeta_n) - \zeta_n \cos(a_2 \zeta_n) \sin(a_2 \zeta'_m)) \\ / (\zeta_m'^2 - \zeta_n^2), & \text{if } \zeta'_m \neq \zeta_n. \end{cases}
\end{aligned} \tag{72}$$

$$\begin{aligned}
V'_{mn} &= \int_0^{a_1} (\sinh(i\bar{\eta}'_n y) / \sinh(i\bar{\eta}'_n b_1)) \cos(-n\pi) \bar{\Phi}_n(y) dy \\
&= \begin{cases} -(\cos(a_1 \gamma_m) \sinh(a_1 \gamma_m) - \cosh(a_1 \gamma_m) \sin(a_1 \gamma_m)) / (2\gamma_m) \\ \sinh(i\bar{\eta}'_n b_1) \cos(-n\pi), & \text{if } \gamma_m = i\bar{\eta}'_n, \\ -i(\gamma_m \cos(a_1 \gamma_m) \sin(a_1 \bar{\eta}'_n) i - \bar{\eta}'_n \sin(a_1 \gamma_m) \cos(a_1 \bar{\eta}'_n) i) \\ / (\gamma_m^2 - \bar{\eta}'_n{}^2) \sinh(i\bar{\eta}'_n b_1) \cos(-n\pi), & \text{if } \gamma_m \neq i\bar{\eta}'_n. \end{cases}
\end{aligned} \tag{73}$$

$$\begin{aligned}
W'_{mn} &= \int_{-a_2}^0 (\cosh(i\bar{\lambda}_n x) / \cosh(-i\bar{\lambda}_n b_2)) \sin((2n+1)\pi/2) \cos \eta_m(x) dx \\
&= \begin{cases} a_2 / \cosh(-i\bar{\lambda}_n b_2) \sin((2n+1)\pi/2), & \text{if } i\bar{\lambda} = \eta_m = 0, \\ (\sin(a_2 \eta_m (1-1i))(1+1i) + \sin(a_2 \eta_m (1+1i))(1-1i)) / (4\eta_m) \\ / \cosh(-i\bar{\lambda}_n b_2) \sin((2n+1)\pi/2), & \text{if } i\bar{\lambda} = \eta_m \neq 0, \\ (\eta_m \cos(a_2 \lambda_n) \sin(a_2 \eta_m) - \lambda_n \cos(a_2 \eta_m) \sin(a_2 \lambda_n)) / (\eta_m^2 - \lambda_n^2) \\ / \cosh(-i\bar{\lambda}_n b_2) \sin((2n+1)\pi/2), & \text{if } i\bar{\lambda} \neq \eta_m. \end{cases}
\end{aligned} \tag{74}$$

$$\begin{aligned}
Q'_{mn} &= \int_0^{a_1} (\cosh(i\bar{\zeta}_n y) / \cosh(i\bar{\zeta}_n b_1)) \sin(-(2n+1)\pi/2) \cos \beta_m(y) dy \\
&= \begin{cases} a_1 / \cosh(i\bar{\zeta}_n b_1) \sin(-(2n+1)\pi/2), & \text{if } \beta_m = \bar{\zeta}_n = 0, \\ \sin(a_1 \beta_m (1-1i))(1+1i) + \sin(a_1 \beta_m (1+1i))(1-1i) \\ / (4\beta_m) / \cosh(i\bar{\zeta}_n b_1) \sin(-(2n+1)\pi/2), & \text{if } \beta_m = \bar{\zeta}_n \neq 0, \\ (\beta_m \cos(a_1 \zeta_n) \sin(a_1 \beta_m) - \bar{\zeta}_n \cos(a_1 \beta_m) \sin(a_1 \bar{\zeta}_n)) \\ / (\beta_m^2 - \bar{\zeta}_n^2) / \cosh(i\bar{\zeta}_n b_1) \sin(-(2n+1)\pi/2), & \text{if } \beta_m \neq \bar{\zeta}_n. \end{cases}
\end{aligned} \tag{75}$$

$$\begin{aligned}
O'_{mn} &= \int_{-a_2}^0 (\sinh(i\bar{\alpha}_n x) / \sinh(-i\bar{\alpha}_n(b_2))) \cos(n\pi) \sin \zeta'_m(x) dx \\
&= \begin{cases} -(\cos(a_2 \zeta_m) \sinh(a_2 \zeta_m) - \cosh(a_2 \zeta_m) \sin(a_2 \zeta_m)) / (2\zeta_m) \\ \sinh(-i\bar{\alpha}_n(b_2)) \cos(n\pi), & \text{if } i\bar{\alpha} = \zeta'_m \neq 0, \\ -(\bar{\alpha}_n \cos(a_2 \bar{\alpha}_n) \sin(a_2 \zeta_m) i - \zeta_m \cos(a_2 \zeta_m) \sin(a_2 \bar{\alpha}_n) i) \\ / (\bar{\alpha}_n^2 - \zeta_m^2) \sinh(-i\bar{\alpha}_n(b_2)) \cos(n\pi), & \text{if } i\bar{\alpha} \neq \zeta'_m \end{cases}
\end{aligned} \tag{76}$$

C The result of the decomposition using symmetry

Using the formula (11), we can compute the complete solutions for the incident wave that is symmetric about $y = 0$ to obtain

$$\phi^{\mathcal{N}}(x, y) = \begin{cases} e^{i\bar{\beta}_p(x+b_2)} \cos \beta_p(y) + \sum_{n=0}^{\infty} \left(\frac{A_n^{\mathcal{N}\mathcal{N}} + A_n^{\mathcal{D}\mathcal{N}}}{2} \right) e^{-i\bar{\beta}_n(x+b_2)} \cos \beta_n(y), & \text{if } x \leq -b_2; \\ \sum_{n=0}^{\infty} \left(\frac{B_n^{\mathcal{N}\mathcal{N}}}{2} \left(\frac{\cosh(i\bar{\alpha}_n x)}{\cosh(-i\bar{\alpha}_n b_2)} \right) + \frac{B_n^{\mathcal{D}\mathcal{N}}}{2} \left(\frac{\sinh(i\bar{\alpha}_n x)}{\sinh(-i\bar{\alpha}_n b_2)} \right) \right) \cos \alpha_n(y), & \text{if } -b_2 < x < 0, \\ \sum_{n=0}^{\infty} \frac{C_n^{\mathcal{N}\mathcal{N}}}{2} \left(\frac{\cosh(i\bar{\eta}'_n y)}{\cosh(i\bar{\eta}'_n b_1)} \right) \cos \eta'_n(x) + \sum_{n=0}^{\infty} \frac{C_n^{\mathcal{D}\mathcal{N}}}{2} \left(\frac{\cosh(i\bar{\zeta}_n y)}{\cosh(i\bar{\zeta}_n b_1)} \right) \sin \zeta_n(x), & \text{if } 0 < x < b_2, \\ \sum_{n=0}^{\infty} \frac{D_n^{\mathcal{N}\mathcal{N}}}{2} e^{i\bar{\eta}_n(y-b_1)} \cos \eta_n(x) + \sum_{n=0}^{\infty} \frac{D_n^{\mathcal{D}\mathcal{N}}}{2} e^{i\bar{\zeta}_n(y-b_1)} \sin \zeta'_n(x), & \text{if } y \geq b_1, \\ \sum_{n=0}^{\infty} \frac{D_n^{\mathcal{N}\mathcal{N}}}{2} e^{i\bar{\eta}_n(-y-b_1)} \cos \eta_n(x) + \sum_{n=0}^{\infty} \frac{D_n^{\mathcal{D}\mathcal{N}}}{2} e^{i\bar{\zeta}_n(-y-b_1)} \sin \zeta'_n(x), & \text{if } y \leq b_1, \\ \sum_{n=0}^{\infty} \left(\frac{A_n^{\mathcal{N}\mathcal{N}} - A_n^{\mathcal{D}\mathcal{N}}}{2} \right) e^{-i\bar{\gamma}_n(-x+b_2)} \sin \gamma_n(y), & \text{if } x \geq b_2. \end{cases}$$

By using the formula (12), we can compute the solutions for the incident wave that is antisymmetric about $y = 0$ to obtain

$$\phi^{\mathcal{D}}(x, y) = \begin{cases} e^{i\bar{\gamma}_p(x+b_2)} \sin(\gamma_p y) + \sum_{n=0}^{\infty} \left(\frac{A_n^{\mathcal{D}\mathcal{D}} + A_n^{\mathcal{N}\mathcal{D}}}{2} \right) e^{-i\bar{\gamma}_n(x+b_2)} \sin(\gamma_n y), & \text{if } x < -b_2; \\ \sum_{n=0}^{\infty} \left(\frac{B_n^{\mathcal{D}\mathcal{D}}}{2} \left(\frac{\cosh(i\bar{\lambda}_n x)}{\cosh(-i\bar{\lambda}_n b_2)} \right) + \frac{B_n^{\mathcal{N}\mathcal{D}}}{2} \left(\frac{\sinh(i\bar{\lambda}_n x)}{\sinh(-i\bar{\lambda}_n b_2)} \right) \right) \sin(\lambda_n y), & \text{if } -b_2 < x < 0, \\ \sum_{n=0}^{\infty} \frac{C_n^{\mathcal{D}\mathcal{D}}}{2} \left(\frac{\sinh(i\bar{\eta}'_n y)}{\sinh(i\bar{\eta}'_n b_1)} \right) \cos(\eta'_n x) + \sum_{n=0}^{\infty} \frac{C_n^{\mathcal{N}\mathcal{D}}}{2} \left(\frac{\sinh(i\bar{\zeta}_n y)}{\sinh(i\bar{\zeta}_n b_1)} \right) \sin(\zeta_n x), & \text{if } 0 < x < b_2, \\ \sum_{n=0}^{\infty} \frac{D_n^{\mathcal{D}\mathcal{D}}}{2} e^{i\bar{\eta}_n(y-b_1)} \cos(\eta_n x) + \sum_{n=0}^{\infty} \frac{D_n^{\mathcal{N}\mathcal{D}}}{2} e^{i\bar{\zeta}_n(y-b_1)} \sin(\zeta'_n x), & \text{if } y > b_1, -a_2 < x < a_2, \\ -\sum_{n=0}^{\infty} \frac{D_n^{\mathcal{D}\mathcal{D}}}{2} e^{i\bar{\eta}_n(-y-b_1)} \cos(\eta_n x) + \sum_{n=0}^{\infty} \frac{D_n^{\mathcal{N}\mathcal{D}}}{2} e^{i\bar{\zeta}_n(-y-b_1)} \sin(\zeta'_n x), & \text{if } y < -b_1, -a_2 < x < a_2, \\ \sum_{n=0}^{\infty} \left(\frac{A_n^{\mathcal{D}\mathcal{D}} - A_n^{\mathcal{N}\mathcal{D}}}{2} \right) e^{-i\bar{\gamma}_n(-x+b_2)} \sin(\gamma_n y), & \text{if } x > b_2. \end{cases}$$

References

- [1] K. F. Riley, M. P. Hobson, and S. J. Bence. *Mathematical methods for physics and engineering: A comprehensive guide*. Cambridge University Press, 3 edition, 2006.
- [2] C. C. Mei, M. A. Stiassnie, and D. K.-P. Yue. *Theory and Applications of Ocean Surface Waves: Part 1: Linear Aspects*. World Scientific, 2005.
- [3] C.J. Chapman. Sound and structural vibration: Radiation, transmission and response. *Journal of Sound and Vibration*, 312:360–361, 2008.
- [4] M. L. Munjal. *M. L. Munjal - Acoustics of Ducts and Mufflers With Application to Exhaust and Ventilation System Design*. John Wiley and Son, 1987.
- [5] M. ul Hassan, M. H. Meylan, and M. Naz. Symmetry, validation, and scattering matrices for time-domain scattering in waveguides. *Applied Mathematical Modelling*, 60:370–383, 2018.
- [6] J. B. Lawrie. Analytic mode-matching for acoustic scattering in three dimensional waveguides with flexible walls: Application to a triangular duct. *Wave Motion*, 50:542–557, 2013.
- [7] L. Girier, M. Roger, H. Bériot, A. Lafitte, and H. Posson. A two-dimensional model of sound transmission through curved and staggered OGV: Effect of inter-vane channel mode transitions. In *25th AIAA/CEAS Aeroacoustics Conference*. American Institute of Aeronautics and Astronautics, 5 2019.
- [8] J. B. Lawrie and R. Kirby. Mode-matching without root-finding: Application to a dissipative silencer. *The Journal of the Acoustical Society of America*, 119(4):2050–2061, 2006.

- [9] M. H. Meylan, L. G. Bennetts, and M. A. Peter. Water-wave scattering and energy dissipation by a floating porous elastic plate in three dimensions. *Wave Motion*, 70:240–250, 2017.
- [10] M. ul Hassan, M. H. Meylan, and M. A. Peter. Water-wave scattering by submerged elastic plates. *The Quarterly Journal of Mechanics and Applied Mathematics*, 62:321–344, 2009.
- [11] R. A. Dalrymple and P.A. Martin. Water waves incident on an infinitely long rectangular inlet. *Applied Ocean Research*, 18:1–11, 1996.
- [12] Y. Hameş and I. H. Tayyar. Plane wave diffraction by dielectric-loaded thick-walled parallel-plate impedance waveguide. *Progress in Electromagnetics Research*, 44:143–167, 2004.
- [13] M. Roger, B. François, and S. Moreau. Cascade trailing-edge noise modeling using a mode-matching technique and the edge-dipole theory. *Journal of Sound and Vibration*, 382:310–327, 2016.
- [14] H. Afsar, G. Peiwei, M. Aldandani, Y. Akbar, and M. M. Alam. Analyzing the acoustic wave propagation characteristics in discontinuous bifurcated waveguide. *Chaos, Solitons and Fractals*, 172, 2023.
- [15] H. Afsar and Y. Akbar. Energy distribution of bifurcated waveguide structure with planar and non-planar surfaces. *Mathematics and Mechanics of Solids*, 28:1155–1169, 2023.
- [16] H. Afsar, G. Peiwei, T. Nawaz, and M. M. Alam. Modeling of silencer by using various porous materials in a trifurcated waveguide structure. *Communications in Nonlinear Science and Numerical Simulation*, 128, 2024.
- [17] M. ul Hassan, M. H. Meylan, A. Bashir, and M. Sumbul. Mode matching analysis for wave scattering in triple and pentafurcated spaced ducts. *Mathematical Methods in the Applied Sciences*, 39(11):3043–3057, 2016.
- [18] M. ul Hassan. Wave scattering by soft-hard three spaced waveguide. *Applied Mathematical Modelling*, 38(17-18):4528–4537, 2014.
- [19] M. ul Hassan and M. Naz. Reflection coefficient of a dominant mode in a pentafurcated duct. *Boundary Value Problems*, 2017, 2017.
- [20] M. ul Hassan, M. Naz, and R. Nawaz. Reflected field analysis of soft-hard pentafurcated waveguide. *Advances in Mechanical Engineering*, 9(5), 2017.
- [21] A. Khalid, S. Younas, I. Khan, R. Manzoor, Rabnawaz, and E. S. M. Sherif. Mode-matching analysis for two-dimensional acoustic wave propagation in a trifurcated lined duct. *Journal of Interdisciplinary Mathematics*, 22(7):1095–1112, 2019.
- [22] T. Nawaz, M. Afzal, and R. Nawaz. The scattering analysis of trifurcated waveguide involving structural discontinuities. *Advances in Mechanical Engineering*, 11(7), 2019.
- [23] S. W. Lee, W.R. Jones, and J.J. Campbell. Convergence of numerical solutions of iris-type discontinuity problems. *IEEE Transactions on Microwave Theory and Techniques*, 19:528–536, 1971.
- [24] L. Lewin. On the inadequacy of discrete mode-matching techniques in some waveguide discontinuity problems. *IEEE Transactions on Microwave Theory and Techniques*, 18:364–369, 1970.
- [25] H. Afsar, G. Peiwei, N. Wu, and M. M. Alam. A study on attenuation patterns of acoustic waves in waveguide structures with flexural boundaries. *JVC/Journal of Vibration and Control*, 2024.
- [26] M. Afzal, R. Nawaz, M. Ayub, and A. Wahab. Acoustic scattering in flexible waveguide involving step discontinuity. *PLoS ONE*, 9(8):103807, 2014.
- [27] H. Afsar, R. Nawaz, and A. Yaseen. Scattering through a flexural trifurcated waveguide by varying the material properties. *Physica Scripta*, 96, 2021.
- [28] H. Bilal and M. Afzal. On the extension of the mode-matching procedure for modeling a wave-bearing cavity. *Mathematics and Mechanics of Solids*, 27:348–367, 2022.
- [29] J. U. Satti, M. Afzal, and R. Nawaz. Scattering analysis of a partitioned wave-bearing cavity containing different material properties. *Physica Scripta*, 94(11), 2019.
- [30] S. Boral, M. H. Meylan, T. Sahoo, and B. Y. Ni. Time-dependent flexural gravity wave scattering due to uneven bottom in the paradigm of blocking dynamics. *Physics of Fluids*, 35, 2023.
- [31] M. Afzal, R. Nawaz, and A. Ullah. Attenuation of dissipative device involving coupled wave scattering and change in material properties. *Applied Mathematics and Computation*, 290:154–163, 2016.
- [32] R. Nawaz and J. B. Lawrie. Scattering of a fluid-structure coupled wave at a flanged junction between two flexible waveguides. *The Journal of the Acoustical Society of America*, 134(3):1939–1949, 2013.
- [33] D.P. Warren, J.B. Lawrie, and I.M. Mohamed. Acoustic scattering in waveguides that are discontinuous in geometry and material property. *Wave Motion*, 36(2):119–142, 2002.

- [34] M. H. Meylan, M. ul Hassan, and A. Bashir. Extraordinary acoustic transmission, symmetry, blaschke products and resonators. *Wave Motion*, 74:105–123, 2017.
- [35] L. Christie and P. Mondal. Mode matching method for the analysis of cascaded discontinuities in a rectangular waveguide. *Procedia Computer Science*, 93:251–258, 2016.
- [36] H. Ali, M. ul Hassan, A. Akgül, and A. Saleh Alshomrani. Wave scattering through step down cascading junctions. *Mathematics*, 11(9), 2023.
- [37] T. Lawrie, S. Gnutzmann, and G. Tanner. Closed form expressions for the green’s function of a quantum graph—a scattering approach. *Journal of Physics A: Mathematical and Theoretical*, 56, 11 2023.
- [38] T. Lawrie, G. Tanner, and D. Chronopoulos. A quantum graph approach to metamaterial design. *Scientific Reports*, 12, 2022.
- [39] M. H Meylan. Time-dependent motion of a floating circular elastic plate. *Fluids*, 6, 2021.
- [40] Ben Wilks, Michael H. Meylan, Fabien Montiel, and Sarah Wakes. Generalised eigenfunction expansion and singularity expansion methods for canonical time-domain wave scattering problems. *Wave Motion*, 132:103421, 2025.
- [41] B. Wilks, M. H. Meylan, F. Montiel, and S. Wakes. Generalized eigenfunction expansion and singularity expansion methods for two-dimensional acoustic time-domain wave scattering problems. *Proceedings of the Royal Society A: Mathematical, Physical and Engineering Sciences*, 480(2297):20230845, 2024.